VILNIUS UNIVERSITY

CENTER FOR PHYSICAL SCIENCES AND TECHNOLOGY

JELENA KOVGER

STUDY ON TITANIUM ANODIC FILMS DECORATION WITH VISIBLE LIGHT ABSORBING SEMICONDUCTOR NANOSTRUCTURES

Summary of doctoral dissertation

Physical sciences, chemistry (03 P)

Vilnius 2017

The research has been carried out at the Institute of Chemistry of Center for Physical Sciences and Technology during the period of 2012 - 2016.

Scientific supervisor: Dr. Arūnas Jagminas (Center for Physical Sciences and Technology, Physical sciences, Chemistry – 03 P).

Evaluation Board:

Chairman – Prof. Habil. Dr. Rimantas Ramanauskas (Center for Physical Sciences and Technology, Physical sciences, Chemistry – 03 P).

Members:

Dr. Renata Butkutė (Center for Physical Sciences and Technology, Technological sciences, Materials engineering – 08 T, Materials Technology – T 150),

Habil. Dr. Zenonas Jusys (Ulm University, Physical sciences, Chemistry – 03 P),

Prof. Habil. Dr. Arūnas Ramanavičius (Vilnius University, Physical sciences, Chemistry – 03 P),

Prof. Dr. Rimantas Raudonis (Vilnius University, Physical sciences, Chemistry – 03 P).

The official discussion will be held at 2 p.m. on the 19th of September, 2017 at a public meeting of the Evaluation Board at the Auditorium of National Center for Physical Sciences and Technology.

Address: Saulėtekio av. 3, LT – 10257 Vilnius, Lithuania.

The summary of doctoral dissertation was mailed on the 31 of July, 2017.

The dissertation is available at the Library of Vilnius University, Library of CPST and online: *www.vu.lt/lt/naujienos/ivykiu-kalendorius.*

VILNIAUS UNIVERSITETAS

FIZINIŲ IR TECHNOLOGIJOS MOKSLŲ CENTRAS

JELENA KOVGER

TITANO ANODINIŲ PLĖVELIŲ DEKORAVIMO MATOMĄ ŠVIESĄ SUGERIANČIAIS PUSLAIDININKIŲ NANODARINIAIS TYRIMAS

Daktaro disertacijos santrauka

Fiziniai mokslai, Chemija (03 P)

Vilnius 2017

Disertacija parengta 2012-2016 metais Fizinių ir technologijos mokslų centre Elektrocheminės medžiagotyros skyriuje.

Mokslinis vadovas – dr. Arūnas Jagminas (Fizinių ir technologijos mokslų centras, fiziniai mokslai, chemija – 03 P).

Disertacija ginama viešame Gynimo tarybos posėdyje:

Pirmininkas – prof. habil. dr. Rimantas Ramanauskas (Fizinių ir technologijos mokslų centras, fiziniai mokslai, chemija – 03 P).

Nariai:

dr. Renata Butkutė (Fizinių ir technologijos mokslų centras, technologijos mokslai, medžiagų inžinerija – 08T, medžiagų technologija – T 150),
habil. dr. Zenonas Jusys (Ulmo universitetas, fiziniai mokslai, chemija 03 – P),
prof. habil. dr. Arūnas Ramanavičius (Vilniaus universitetas, fiziniai mokslai, chemija – 03 P),
prof. dr. Rimantas Raudonis (Vilniaus universitetas, fiziniai mokslai, chemija – 03 P).

Disertacija bus ginama viešame Gynimo tarybos posėdyje 2017 m. rugsėjo mėn. 19 d. 14 val. Nacionalinio fizinių ir technologijos mokslų centro salėje.
Adresas: Saulėtekio al. 3, LT – 10257 Vilnius, Lietuva.

Disertacijos santrauka išsiuntinėta 2017 m. liepos mėn. 31 d.

Disertaciją galima peržiūrėti Fizinių ir technologijos mokslų centro ir Vilniaus universiteto bibliotekose, bei VU interneto svetainėje adresu: *www.vu.lt/lt/naujienos/ivykiu-kalendorius.*

1. INTRODUCTION

Researches on replacement of fossil fuels by renewable sources utilising solar, wind or hydro energy is particularly relevant nowadays, as ecological, political and economic factors contribute towards this change. The main attention in this research is given to solar and fuel cells, that convert solar energy into electrical and chemical energy, respectively, with conversion efficiency of up to 20%. The prediction written down on the walls of Brussels airport, that solar power driven aircraft is going to be created, may not only come true as an experiment, but will be commercially available to transfer people in the nearest future.

New nanostructure materials, their order colonies, layered films, synthesis and construction of heterostructures allow scientists to develop new or materials of improved properties that will determine the future of scientific and technological progress. Currently, nanostructured silicon-SiO_2 junctions are the most efficient transportation medium of solar energy. However, great efforts are also directed to formation and research of the heterostructures of new photoactive materials and thin films, such as perovskites, cassiterites, and optically transparent oxides (TiO_2, ZnO, Fe_2O_3).

Optical properties of the above-mentioned oxide films and nanostructured layers are being studied for the second decade. Seeking to create more effective absorbers, much of attention currently is directed to the search of new heterostructures and its cognition. There are plenty of studies intended for formation of {101} and {001} faceted anatase-TiO_2 crystal layers, their doping with other metals and metalloids, dyeing with organic dyes, and decorating with nanoparticles of other semiconductors. The target of these researches is to expand sunlight absorption region. Although progress has been achieved using these methods, they are rather time-consuming, environmentally unfriendly and energy wasteful. Therefore, search and research of new nanostructured TiO_2 layers and composites with nanoparticles of other semiconductors based on their environmental friendliness, low costs, and chemical resistance may provide a new strategy for designing more efficient TiO_2-based photo and electrocatalysts.

For doping of TiO_2 thin layers, as well as for its decoration, laser ablation, magnetron sputtering, and chemical or light-initiated reduction techniques have been

proposed. Meanwhile, the electrolytic decoration of nanoporous TiO_2 films formed on Ti surface in anodic oxidation path, has received much less attention.

The aim of the work was

Investigate the possibilities of anodic TiO_2 film nanotubes for electrochemical decoration of lower band gap semiconductor nanoparticles.

The main tasks of the work are the following:

- Optimize titanium surface anodizing conditions for formation of nanotubed morphology, self-organized, anatase-structured TiO_2 films.
- Investigate the regularities of electroforming of copper oxides and selenides nanoparticles in TiO_2 nanotubes.
- Investigate the impact of doping $Ti|TiO_2$ junction with hydrogen on characteristics of electro formation of semiconductor nanoparticles in nanotubes and its control.
- Investigate optical properties of anatase-TiO_2 films decorated with copper oxide and selenide nanoparticles.
- Investigate together options of hydrothermal synthesis of MoS_2 nanostructures and decorating of TiO_2 films with them, choosing compositions of solutions and synthesis conditions. Evaluate catalytic properties of the created $Ti/TiO_2 – MoS_2$ electrodes for the hydrogen extraction from water solution.

Novelty of scientific investigation:

- Selected and optimized aqueous electrolyte compositions for easy-controlled and uniform decoration of anatase-TiO_2 film nanotubes (Ntb) with copper suboxide and selenide nanoparticles using alternating current.
- For the first time, the decorating path of anodic TiO_2 film nanotubes with superionic $Cu_{1.75}Se$ nanoparticles is presented.
- TiO_2-based hetero structures, electrochemically decorated with nanoparticles of a lower band gap semiconductor allows significant expansion of absorbed Solar light region towards visible light.
- For the first time, there is demonstrated that by doping of $Ti|TiO_2$ electrode with hydrogen the electrical conductivity of TiO_2 Ntbs increases at least 6 orders of

magnitude due to a “spilt over” effect, that allows uniform electrochemical decoration of TiO_2 Ntb walls with both copper suboxide and selenide nanoparticles.

- For the first time, for uniform decoration of anodized Ti electrodes, as well as oxide film Ntbs with nanoplatelet MoS_2 species, the hydrothermal approach has been used showing that Ti/TiO_2 Ntb-MoS_2 electrodes catalyse hydrogen evolution reaction from water solutions.

Statements for defence:

1. The surfaces of anodic TiO_2 film nanotubes can be uniformly decorated with semiconducting copper suboxide and copper selenide nanoparticles in aqueous electrolytes using alternating current (AC) deposition path.

2. The doping of Ti|TiO_2 Ntb electrode with hydrogen results in its electrical conductivity increase by 6 orders of magnitude and more, enabling decorating of TiO_2 Ntb surface with Cu_2O, Cu_3Se_2 and $Cu_{2-x}Se$ nanoparticles uniformly and predictable, using AC electrodeposition way.

3. Due to synergetic activities, the self-ordered anatase TiO_2 Ntb films, decorated with nanoparticles of lower band gap semiconductors, absorb a significantly wider sunlight spectrum region.

4. Uniform decoration of Ti/TiO_2 Ntbs with nanoplatelet MoS_2 species can be obtained via hydrothermal treatment at the optimized conditions. Obtained heterostructures can be used for catalytical H_2 production from water.

2. EXPERIMENTAL

2.1. Electrochemical formation of TiO_2 Ntb films

Ti foil at 99.7% purity and 0.127-mm-thick, purchased from Aldrich, was used to prepare the specimens at the size of 12 × 12 mm^2. The surface of samples was ultrasonically cleaned in acetone, ethanol, and water, for 6 min in each substance, air dried, and anodized in the thermostated ethylene glycol (Etg) solution containing 0.3 wt% NH_4F and 20 mL L^{-1} H_2O at 20 ± 0.5 °C, then 50 and/or 30 V was applied using DC power supply for 20 to 120 min. These conditions have been reported for most ordering nanotubed titania films formation. In some cases of anodizing at 50 V, to decrease the thickness of titania barrier layer, the anodizing voltage (E_a) was step-wise

decreased at the end of anodizing down to 30 V at a rate of 1.0 V min^{-1}. Two platinum plates, used as cathodes, were maintained at a distance of ~ 13 mm from the Ti specimen. Each sample was anodized in a fresh solution. After anodizing, the specimens with TiO_2 Ntb film coated on both sides were taken out of the bath, ultrasonically agitated in ethylene glycol for 5 s to remove the debris from the surface, washed well with distilled water, and air dried. Resulting film was calcined in air at 450 °C for 2 h using 10 °C min^{-1} ramp and subjected to further treatments.

2.2. Decoration of TiO_2 Ntb surface with Cu_2O species

Electrodeposition of Cu_2O on TiO_2 nanotube walls was accomplished in a two-electrode glass cell, 200 mL in volume, containing aqueous solution of 0.1 mol L^{-1} copper acetate, $Cu(CH_3COO)_2 \cdot H_2O$, 0.1 mol L^{-1} magnesium acetate, $Mg(CH_3COO)_2 \cdot 4H_2O$, and acetic acid to maintain pH at 5.3. Several graphite stripes connected and positioned around the working specimen were used as the counter electrode. All electrodepositions were carried out in room temperature solution by alternating current (AC), 50 Hz in frequency, under peak-to-peak voltage ($U_{p\text{-}to\text{-}p}$) or effective current strength control for up to 15 min. All solutions were prepared with deionised water and reagent grade chemicals. After deposition, each sample was thoroughly rinsed and air dried.

2.3. Decoration of TiO_2 Ntb surface with copper selenides

Electrodeposition of copper selenide species was accomplished in a two-electrode glass cell, 200 mL in volume, containing an aqueous solution of 30 mmol L^{-1} copper sulphate, $CuSO_4 \cdot 5H_2O$, 15 mmol L^{-1} selenious acid, H_2SeO_3, 50 mmol L^{-1} magnesium sulphate, $MgSO_4 \cdot 7H_2O$, and sulphuric acid and/or triethanolamine (TEA) to adjust the pH at 1.25 or 5.3, respectively. Several graphite stripes connected and positioned around the working specimen were used as the counter electrode. All electrodepositions were carried out using alternating current, 50 Hz in frequency, under peak-to-peak voltage ($U_{p\text{-}to\text{-}p}$) control for up to 15 min. A Keithley 230 programmable voltage source was used for AC depositions and for electrochemical hydrogen doping of TiO_2 Ntbs. All solutions were prepared with deionized water and reagent grade chemicals. All depositions and AC treatments were carried out at room temperature. After deposition, each sample was thoroughly rinsed with distilled water and air dried.

2.4. Sensitization of TiO_2 Ntb films by hydrogen doping

It is commonly accepted that the resistance of TiO_2 Ntb films is linearly related with the formation voltage: the higher the anodizing voltage, the higher the resistance of resulting film. In this study, to decrease the resistance of TiO_2 Ntbs before deposition tests, three approaches were used: (i) step-wise voltage decrease at the end of anodizing; (ii) hydrogen insertion by AC or DC pretreatment of calcined films in the acidic 0.005 mol L^{-1} H_2SO_4, 0.005 or 0.05 mol L^{-1} H_2SeO_3 or alkaline 0.5 mol L^{-1} KOH solutions for 1 min, and (iii) treating of calcined TiO_2 Ntb films in H_2 atmosphere at 1.5 atm and ambient temperature for 1 h.

2.5. Hydrothermal synthesis of MoS_2 species

For the fabrication of flower-shaped MoS_2 species possessing crystalline structure and few layered 2-D leaflets in the solution bulk as well as inside the TiO_2 Ntb film tubes, the hydrothermal synthesis in the thiourea, $(NH_2)_2CS$, and ammonium heptamolybdate, $(NH_4)_2Mo_7O_{28} \cdot 4H_2O$ solutions was carried out. Analytically pure ammonium heptamolybdate was purchased from REAC EM, Slovakia, whereas thiourea from Sigma. In these investigations a Teflon-lined autoclave of 20 mL capacity was filled to 60 vol % with working solution, the concentration of both precursors in which varied from 0.5 to 15 mmol L^{-1} for $(NH_4)_2Mo_7O_{24}$ and from 9 to 270 mmol L^{-1} for thiourea. The cleaned TiO_2 Ntb specimen was immersed vertically into the solution using a special holder made of Teflon. The autoclave was sealed into a stainless steel tank and the reaction was conducted in the programmable oven Zhermack within 170° to 225 °C temperature range using 10 °/min ramp. Hydrothermal synthesis lasted from one to twenty hours and then the autoclave was cooled to room temperature naturally. After the hydrothermal reaction, as-formed products were carefully rinsed with water and dried. Some specimens were annealed in air or oxygen-free atmosphere by means of heating together with Cu foil in a sealed glass tube at 300 °C for 20 h.

3. RESULTS AND DISCUSSION

3.1. Decoration with Cu_2O nanoparticles

3.1.1. AC treatment

Typical top-side and cross-sectional SEM views of selected TiO_2 Ntb film before and after AC treatments in the Cu(II) acetate solution are shown in Figure 1. From the SEM images the covering of TiO_2 nanotube walls and TiO_2 Ntb film surface with numerous particles can be clearly seen. Note that just after ten minutes of AC treatment at alternating current density (j_{ac}) of 0.35 A dm^{-2} the inner diameter of TiO_2 tubes, 45-50 nm in diameter at the open end, narrowed significantly but remained unclogging.

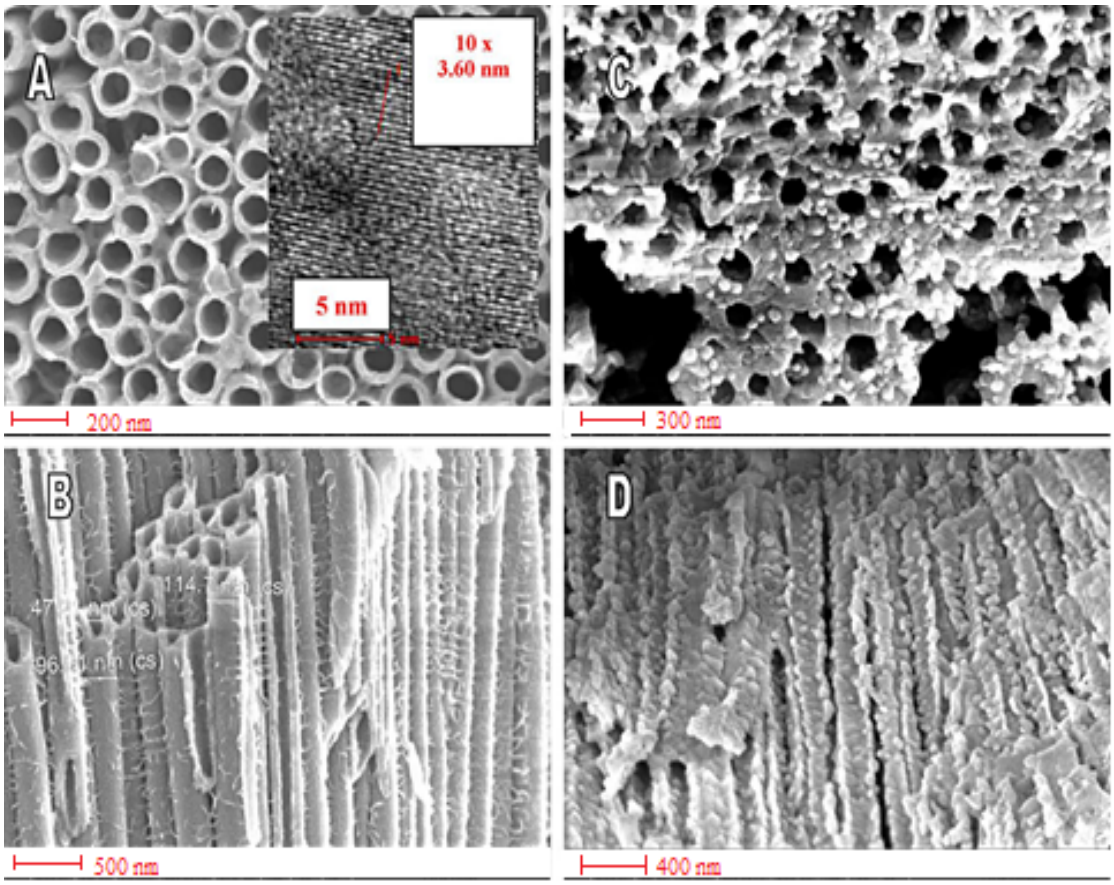

Fig. 1. Top-side (A, C) and cross-sectional (B, D) FESEM views of the TiO_2 Ntb film before (A, B) and after (C, D) AC treatment in the solution containing 0.1 $Cu(CH_3COO)_2$ + 0.1 mol L^{-1} $Mg(CH_3COO)_2$ + CH_3COOH up to pH 5.3 at a constant current density of 0.5 A dm^{-2} for 10 min. TiO_2 Ntb was formed by Ti surface anodizing in the Etg solution containing 0.3 NH_4F and 2.0 wt% H_2O at 50 V for 40 min followed by voltage decrease by 1.0 V min^{-1} down to 30 V and calcination at 500 ºC for 2 h. Inset depicts HRTEM image of pure TiNT film.

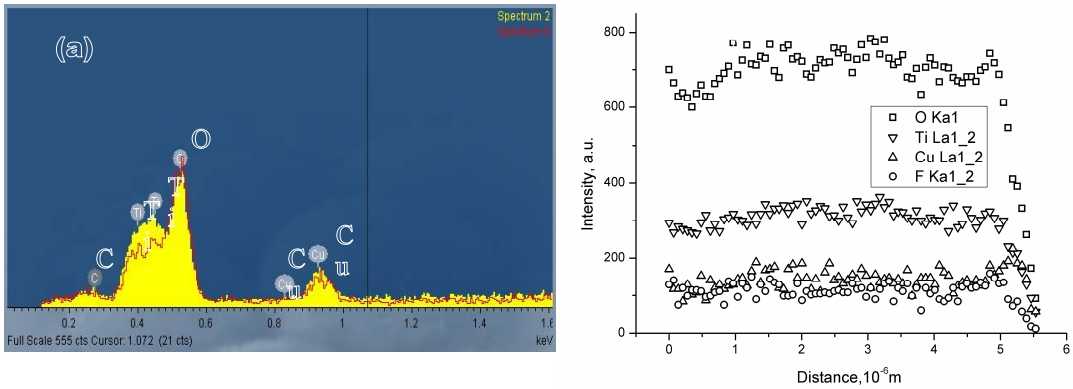

Fig. 2. EDX spectrum of TiO_2 Nt film after 60 c AC decoration in Cu (II) acetate electrolyte (a) and distribution profiles of O, Ti, Cu, and F elements inside the TiO_2 Ntb film in thickness of ≈ 5.5 μm (b).

Again, the content of deposited material and the size of particles can be easily controlled by duration of AC treatment and processing regime. In our studies we employed quite wide range of AC current densities, starting from ~ 0.15 A dm^{-2}, can be applied for depositions. However, in case of j_{ac} ≥0.5 A dm^{-2} and longer deposition times even at j_{ac} ≥ 0.35 A dm^{-2} TiO_2 Ntb films were destroyed in specimen corners and some points and removed from the Ti substrate. The decrease of the thickness of TiO_2 Ntb film barrier layer by anodizing voltage step-wise decrease at the end of film formation results in the prevention of it's detachment from the substrate during subsequent rinsing, drying, calcination, and AC treatment even at high AC densities attaining 1.0 A dm^{-2}. Moreover, the AC treatment results in the quite uniform deposition of nm-scaled species both inside and outside the tubes along the nanotube length approximated 5.5 μm for TiO_2 Ntb films formed during 30 min (Fig. 2). Again, the content of deposited material and the size of species can simple be controlled by AC treatment time and processing regime.

Figure 3a shows a STEM image of the TiO_2 Ntb fragment after 10 min of AC treatment at $U_{p\text{-}to\text{-}p}$= 2.2 V in the Cu(II) acetate solution demonstrating the formation of numerous seeds inside the TiO_2 tube. EDX spectra taken along the cross-section of single nanotube revealed the presence of copper containing species inside and outside the nanotube (Fig. 5b). Going deeper quite uniform incorporation of copper was observed.

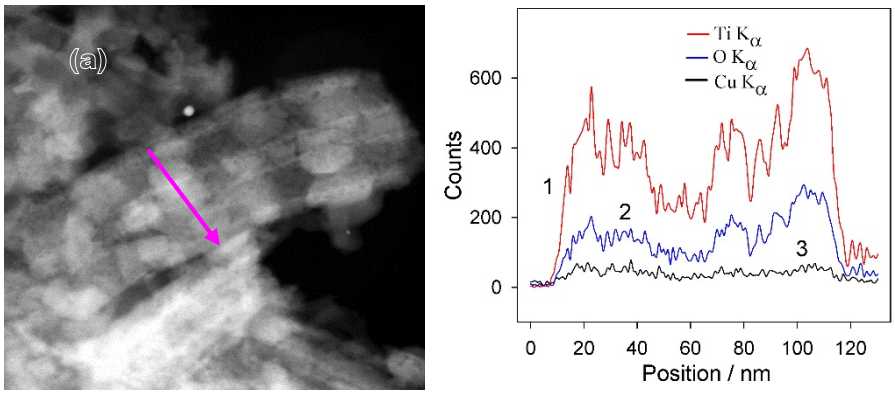

Fig. 3. (a): Scanning transmission electron microscopy (STEM) image of TiO_2 nanotube fragment after AC deposition of Cu_2O at $U_{p\text{-}to\text{-}p}$ = 2.2 V for 10 min. The distribution profiles of Ti (1), O (2) and Cu (3) elements along nanotube cross-section are shown in (b).

3.1.2. Raman investigations

Figure 4 compares Raman spectra of TiO_2 nanotubes before and after deposition of copper containing species. Strong Raman bands at 147, 397, 518, and 637 cm^{-1} are characteristic of crystalline anatase TiO_2 structure. The dominant band at 147 cm^{-1} was assigned to $E_g(1)$ Raman-active mode, while the peaks at 397 and 637 cm^{-1} belongs to $B_{1g}(1)$ and $E_g(3)$ eigenmodes, respectively. The peak near 518 cm^{-1} is composed of two eigenmodes, $B_{1g}(2)$ and A_{1g}, which can be distinguished at lower temperatures.

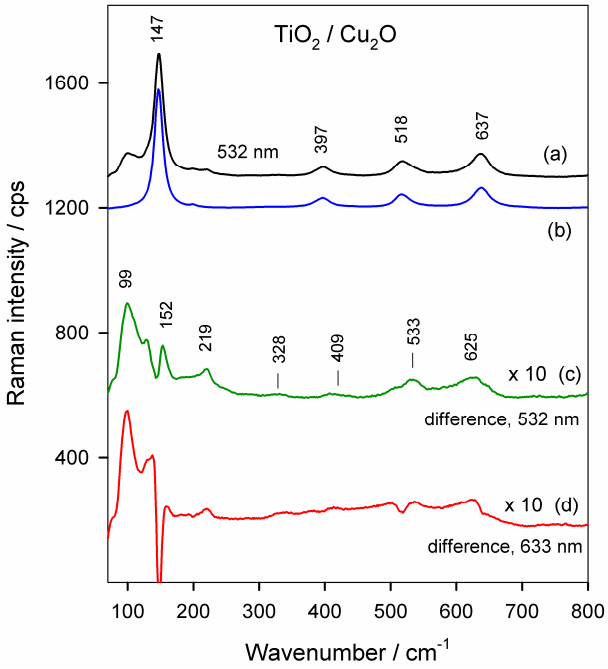

Fig. 4. Raman spectra of (a) TiNT film with deposited Cu_2O and (b) bare TiO_2 Ntb. The difference spectra (c) and (d) are also shown. Excitation wavelengths are 532 nm (a, b, c), and 633 nm (d). Cu_2O deposition current density is 0.4 A dm^{-2}. Spectra were normalized according to intensity of TiO_2 peak at 397 cm^{-1}.

Difference spectrum (Fig. 4c) clearly shows several peaks associated with copper oxygenous compounds. Bands at 219, 533, and 625 cm^{-1} evidence presence of Cu_2O. Cuprous oxide belongs to O_h^4 space group symmetry. Consequently, the optical phonons are distributed by the symmetry as follows:

$$\Gamma_{op} = \Gamma_{15}^{-(1)}(IR) + \Gamma_{15}^{-(2)}(IR) + \Gamma_{25}^{+}(R) + \Gamma_{25}^{-} + \Gamma_{2}^{-} + \Gamma_{12}^{-} \quad (1)$$

The only one Raman active mode (Γ_{25}^{+}) was theoretically predicted at 550 cm^{-1} and observed experimentally near 524–531 cm^{-1}. Thus, relatively broad peak at 533 cm^{-1} in the difference spectrum (Fig. 4c) is associated with Γ_{25}^{+} mode of Cu_2O. The other broad feature at 625 cm^{-1} belongs to infrared active $\Gamma_{15}^{-(2)}$ mode. The relatively narrow peak at 152 cm^{-1} belongs to infrared active $\Gamma_{15}^{-(1)}$ mode. This band was clearly visible in spectroelectrochemical studies of Cu electrode in alkaline solutions and was suggested as a Raman marker of Cu_2O. However, in studies of copper oxygeneous compounds embedded into the TiO_2 nanotubes the strong $E_g(1)$ band from nanotubes at 147 cm^{-1} prevents precise measurement the parameters of this mode (Fig. 4 1a and b). The low intensity feature near 409 cm^{-1} probably belongs to Γ_{12}^{-} mode. The narrow and well-defined band at 219 cm^{-1} is associated with two-phonon scattering of Γ_{2}^{-} mode. While one-phonon Raman scattering for Γ_{2}^{-} mode is forbidden, the two-phonon band is allowed and usually appears as characteristic Raman feature of Cu_2O. Interestingly, intense low frequency band near 99 cm^{-1} is visible in spectrum of copper oxygeneous compounds formed within the TiO_2 nanotubes by AC treatment in Cu(II) acetate solution (Fig. 4c). This band most likely is associated with Γ_{25}^{-} mode, which is expected to be observed based on theoretical analysis at 98.6 cm^{-1}. The intensification of forbidden modes is associated with nanocrystal size effect and presence of defects in the copper oxide structure. Comparison of difference Raman spectra obtained with 532 and 633 nm excitations (Fig. 4c and d) demonstrates some enhancement of Cu_2O bands with lower wavelength excitation. No evidence for presence of CuO phase was obtained by Raman spectroscopy. It was demonstrated that the most intense Raman band of cupric oxide appears near 296 cm^{-1}. No such band was observed in our spectrum (Fig. 4c). Fig. 5

shows typical XRD pattern of the TiO_2 Ntb film AC treated in Cu(II) acetate solution. From this pattern, the TiO_2 Ntb film exhibits a set of diffraction peaks attributable either to anatase-TiO_2 (PDF: 00-021-1272) or Cu_2O (PDF: 01-078-2076). Any peaks can be ascertained to CuO, Cu^0 or $Cu(OH)_2$ were detected.

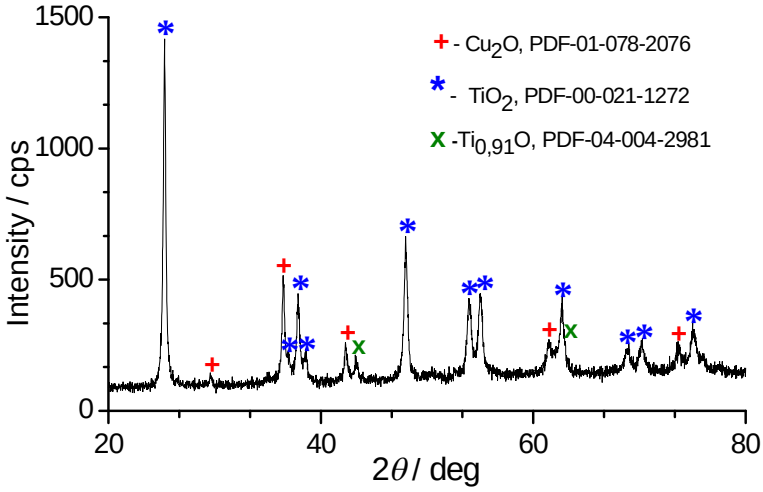

Fig. 5. Typical XRD pattern of the TiO_2 Ntb film AC treated in the Cu(II) acetate solution as in Fig. 1D.

3.1.3. Voltammetric investigations

Annealing of TiO_2 Ntbs with encased cuprous oxide allows easy conversion of Cu_2O to CuO, what can be readily observed from cathodic reduction profiles of the samples. The reduction of Cu_2O species deposited under various AC treatment conditions was performed by scanning the potential from the open-circuit *E* value of TiO_2 Ntb-Cu_2O electrode (approximately +0.75V) to -0.16V and backwards in deaerated solution of 0.1 mol L^{-1} KOH at a rate of 0.2 mV s^{-1}.The reduction of Cu_2O species deposited under various AC treatment conditions was performed by potential scan from the open TiO_2/Cu_2O electrode potential approximated +0.65 V to -0.15 V and backwards in deaerated solution of 0.1 mol L^{-1} KOH at a rate of 0.2 mV s^{-1}. The annealing of such TiO_2 Ntb-Cu_2O heterostructures in air at 250 ºC for several hours resulted only in the crystallization of Cu_2O species (Fig. 6, curve 2) whereas at higher temperatures, particularly at 350-550 ºC, Cu_2O transformed to CuO-Cu_2O mixture with composition depending on the on the annealing temperature, T_{ann}. (Fig. 6, curves 3 to 5). To explain the calcination effects on Cu_2O species anchored onto the TiO_2 Ntb walls, more detail investigations estimating the influence of the content and size of Cu_2O crystallites are required.

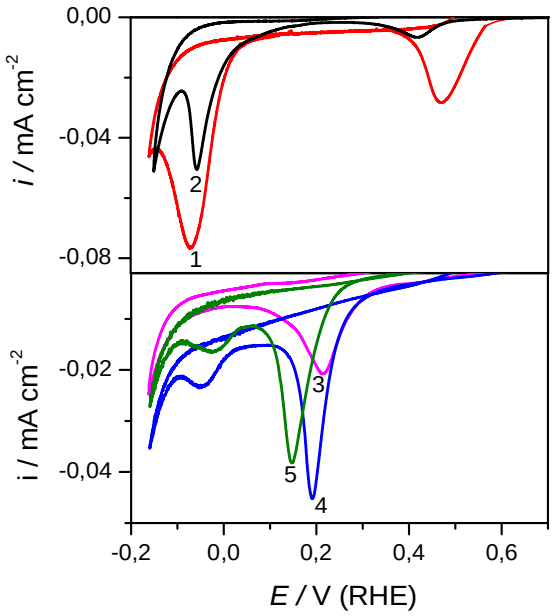

Fig. 6. Reduction profiles for TiO_2 Ntb films grown in Etg electrolyte at 50 V during 40 min with subsequent bath voltage decrease down to 30 V, then calcined, and AC treated in the Cu(II) solution as in Fig. 1 at $U_{p\text{-}to\text{-}p}$ = 1.8 V for 7.5 min (1), annealed again in air at 250º (2); 350º (3), 450º (4) and 550 ºC (5) for 2 hours.

3.1.4. Optical measurements

The optical constants of the bare and Cu_2O-decorated TiO_2 Ntb film were determined in the photon energy range 1.4 to 6.0 eV in order to obtain information about their electronic structures and to compare them. Experimental diffused reflectance spectra were converted to Kubelka-Munk function. The Tauc plot was used for determination of band gap for allowed direct transition for both specimens are presented in Figure 7. On the basis of analysis of possible allowed direct and allowed indirect (not showed here) transitions in TiO_2 Ntb – Cu_2O heterostructures it seems likely that mainly direct transitions are allowed for these films; other model leads to significantly lower absorption edges, ca. around 1.2 eV.

One can see that the diffused reflection spectra on the bare TiO_2 Ntb and TiO_2 Ntb – Cu_2O are similar from the qualitative point of view, although bare TiO_2 Ntb sample demonstrates significantly higher reflection within 300 to 530 nm light wavelength range (Fig. 7a). In addition, the main reflection peak of bare TiO_2 Ntb in the UV region, seen in a vicinity of 395 nm for Cu_2O-decorated TiO_2 Ntbs, is shifted to 365 nm. The Kubelka-Munk function calculated from, [$K = (1\text{-}R_d)^2/2R_d$)], for both specimens are presented in Figure 7b. It is obvious that TiO_2 Ntb-Cu_2O film, demonstrating a broad

absorption peak in the region between 1.5 and 3.3 eV, absorbs much more light than bare TiO_2 Ntb; the difference being very striking for the sharp peak near 2.75 eV.

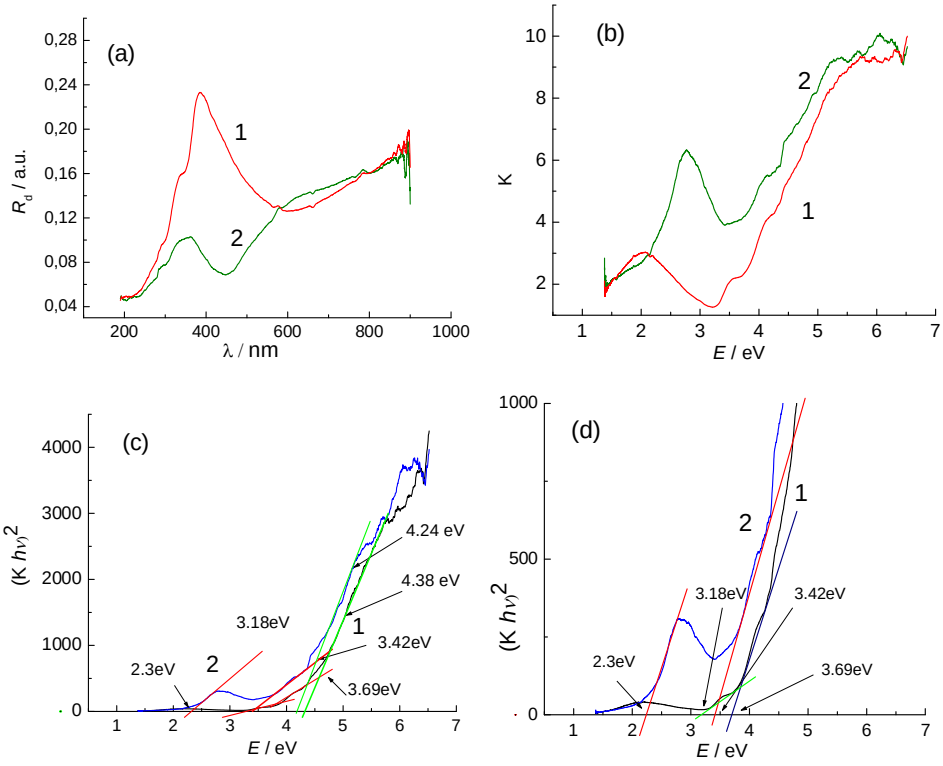

Fig. 7. Typical diffuse reflectance (a) and Kubelka-Munk function (b-d) spectra of bare TiO_2 Ntb film (1) and the-same film encased with Cu_2O nanocrystals (2). In (c)-overview and (d)-low energies range, the absorption edges determined for allowed direct transitions are shown for both specimens.

Analysis of absorption plots for possible allowed direct transitions (Fig. 7 c, d) shows that in the case of TiO_2 Ntb-Cu_2O sample absorption edge typical for bare anatase TiO_2 (~ 3.18 eV) is shifted evidently into the visible range (~ 2.3 eV). The same effect is seen for higher energy subbands in UV region where E_g' = 3.69 eV for bare TiO_2 film is shifted to E_g' = 3.42 eV for TiO_2 Ntb-Cu_2O heterostructure. We suspect that the red-shift and enhancement of the light absorption in the UV-vis region should be attributed to the uniform loading of TiO_2 nanotubes by Cu_2O crystals (see Fig. 3) as well as to profound interaction between Cu_2O and anatase TiO_2.

To obtain more information about optical properties of bare TiO_2 Ntb film and TiO_2 Ntb -Cu_2O heterostructure, the sets of specular reflection (R_s) spectra at various excitation beam angles in the range from 10 to 75° were investigated. Specular reflection of TiO_2 Ntb-Cu_2O film at different angles of light incidence was studied in the spectral

range from 250 to 600 nm by using an ellipsometric stage. Typical R_s *versus* λ plots for TiO_2 Ntb-Cu_2O film are shown in the Inset of Figure 8. Qualitatively, these dependencies are similar to that recorded for bare TiO_2 film although the magnitude of reflections, R_s, at the same angles is about twice higher for bare TiO_2. Furthermore, analysis of reflection intensities at various angles shows that TiO_2 Ntb-Cu_2O heterostructure is characterized by significantly lower dependence of reflection on the excitation light beam angle that could be especially useful in the solar cell contours.

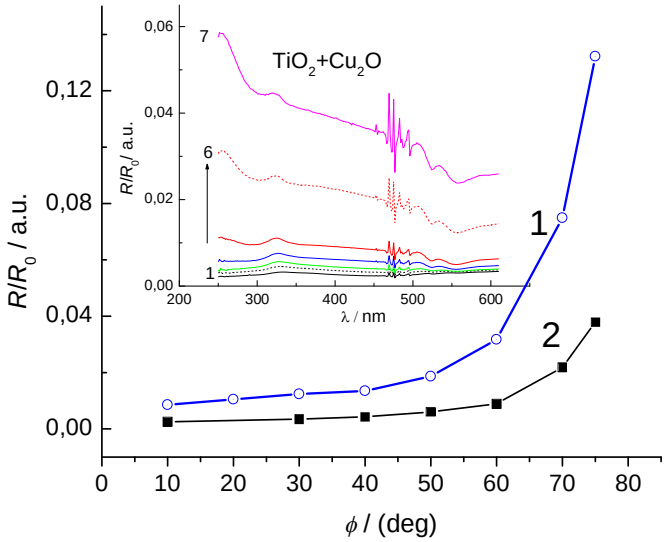

Fig. 8. The dependence of relative intensities of diffused reflections for bare TiO_2 Ntb film (1) and TiO_2 Ntb -Cu_2O (2) on the excitation beam angle calculated from the corresponding R_s *versus* λ spectra, ϕ: 1) 10º, 2) 30º, 3) 40º, 4) 50º, 6) 70º, 7) 75º

Discussion

Uniform deposition of pure Cu_2O species onto surface of TiO_2 Ntb walls in weekly acidic Cu (II) acetate solution by AC treatment (see Fig. 3a) seems a bit surprising. Therefore, to explain the formation of bulk Cu_2O, the material balance analysis of all species can be formed in the tested electrolyte at various pH was performed using Lewenberg-Marquardt interactions approach. As reported in, in the solution of interest Cu^{2+}, $CuAc^+$, $CuAc_2$, and protonated (HAc) species can exist. Variation of their content with pH is presented in Figure 9. In calculations of equilibrium concentrations, the following Pourbaix relations and equilibrium constant of Cu^{2+} and Cu^0 reproportionation reaction:

$$\log[Cu^+]_{max} = -0{,}84 - pH, \quad (2)$$

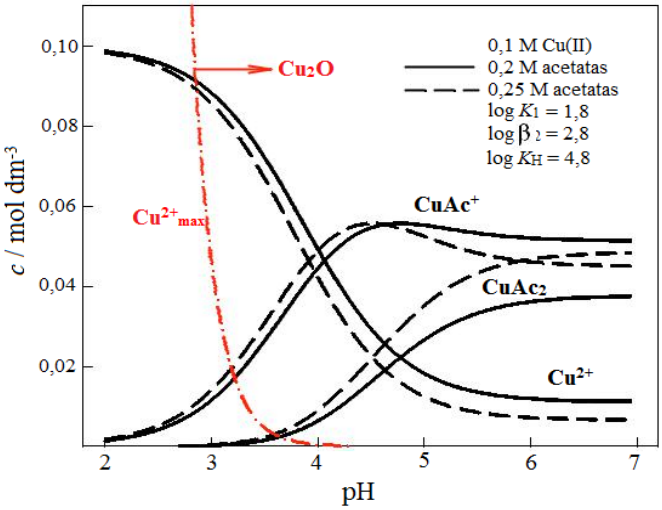

Fig. 9. Variation of the contents of copper-containing species in the 0.1 mol L^{-1} $Cu(OOCCH_3)_2$ + |0.1 mol L^{-1} $Mg(OOCCH_3)_2$ + CH_3COOH solution with pH. Da-dotted line designates the pH value of formation Cu^+ species.

$$Cu^{2+} + Cu^0 \rightleftarrows 2Cu^+, K = 610^{-7} \quad (3)$$

$$\log[Cu^{2+}]_{max} = 4{,}67 - 2pH \quad (4)$$

were used. As can be seen, the deposition of copper in the metallic state only should take place at pH < 3.0, whereas at slightly higher pH values the region of thermodynamically stable Cu_2O formation, if Cu^0 appeared, begins. Therefore, formation of Cu_2O in weekly acidic Cu acetate electrolyte at pH = 5.3 is most plausible *via* formation of Cu^+ according to equation (2) and its subsequent conversion to Cu_2O by reaction:

$$2Cu^+ + 2OH^- \rightarrow Cu_2O(s) + H_2O. \quad (5)$$

It is worth also noting that the potentials of anatase-TiO_2 electrode and Cu^0 surface in the solution used in this study at pH = 5.3 equaled to +0.34 and +0.29 V versus RHE, respectively. It means that Cu^0 being in contact with TiO_2 Ntb wall surface behaves as anode and should be thermodynamically unstable, whereas Cu_2O-stable. Nevertheless more detail research is required to determine the pH region of pure Cu_2O formation.

We also note that in earlier publications direct current treatment of TiO_2 Ntb films in the tin and iron salts solutions resulted in the deposition of metallic dendrites protruding from the titania tubes as shown in the scheme of Figure 10a. Oxidation of these dendrites was performed by subsequent annealing in air. In the present study,

slightly acidic Cu(II) solution and alternating current approach were applied for the direct deposition of pure Cu_2O species onto the TiO_2 Ntb walls in the shape of uniformly distributed numerous nm-sized seeds and, subsequently, particles, as shown by a scheme presented in Figure 10b. We suggest that this unique effect, not yet considered, should be ascribed to the alternating current regime, which prevents the breakdown of titania barrier layer, and as well as to decrease in the resistance of TiO_2 Ntb walls during the initial cathodic pulses due to electrochemical self-doping by reaction $Ti^{4+} + e^- \rightarrow Ti^{3+}$ as suggested, for example.

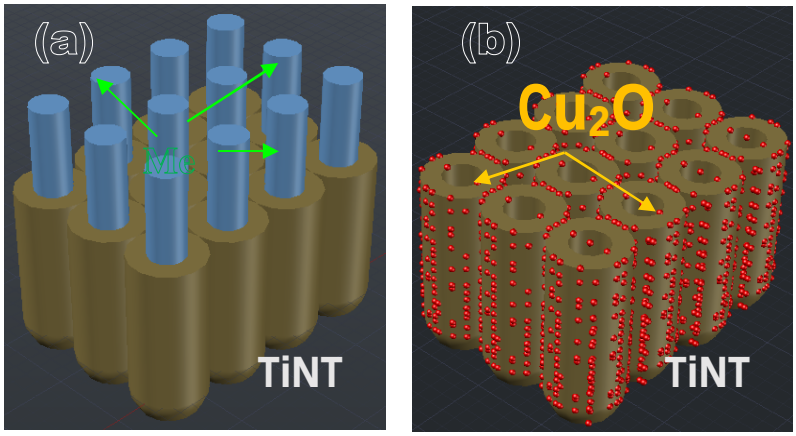

Fig. 10. Schematic illustration of the self-assembled deposition into the TiO_2 nanotubes by direct (a) and alternating (b) current approaches.

The red-shift in E_g value of the n-type TiO_2 Ntb film with increasing content of semiconducting p-type Cu_2O crystallites (E_g = 2.1 – 2.19), tethered to the TiO_2 Ntb walls, should be ascribed to visible light induced charge transfer from Cu_2O to the TiO_2 conduction band, as has been suggested in other recent publications.

We note that uniform decoration of TiO_2 Ntb films with lower band gap semiconducting particles using simple controllable AC deposition method represents promising approach towards fabrication of more efficient solar and fuel cells. Our recent investigations have also shown that TiO_2 Ntb films decorated with Cu_2O nm-sized crystallites demonstrate strong antifungal properties.

3.2. Effect of hydrogen doping on the loading of titania nanotube films with copper selenide species

3.2.1. Characterization of AC depositions inside the as-grown and annealed TiO_2 Ntb film

To determine the location and uniformity of loading of copper selenide species inside the as-grown and annealed TiO_2 Ntb films by AC deposition, we have used SEM–EDS and X-ray mapping investigations. Figure 11 depicts the typical morphology of anatase structure TiO_2 Ntb film after AC treatment in the acidic Cu(II)-H_2SeO_3 solution with pH 1.25. It is reasonable to mention that similar solution has been suggested by us earlier for porous alumina colouring. As seen, in this solution under the constant AC peak-to-peak voltage ($U_{p\text{-}to\text{-}p}$) mode, densely packed crystallites in size of from 60 to 160 nm appear to be deposited mainly at the TiO_2 Ntb film surface. Some quantity of similar in shape but smaller crystallites are also deposited at the bottom part of TiO_2 Ntb film, whereas only a pretty small content is seen in the film bulk.

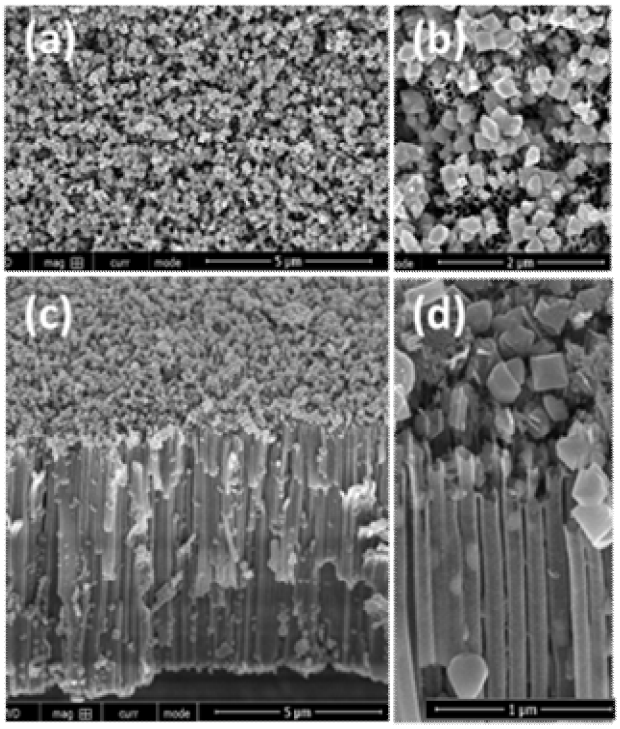

Fig. 11. Top-side (a,b) and cross-sectional (c,d) SEM views of TiO_2 Ntb film encased with copper selenide nanocrystals by alternating current deposition from an aqueous solution containing 30 mmol L^{-1} $CuSO_4 \cdot 5H_2O$, 50 mmol L^{-1} $MgSO_4 \cdot 7H_2O$ and 15 mmol L^{-1} H_2SeO_3 kept at a pH=1.25 at peak-to-peak voltage ($U_{p\text{-}to\text{-}p}$) 1.2 V for 7.5 min.

The quantity of nanocrystallites deposited inside the nanotubes (Fig. 11d), however, is low. Increase in the $U_{p\text{-}to\text{-}p}$ up to 2.2 V resulted in detachment of TiO_2 Ntb film in certain places of the electrode, particularly at the electrode edges.

Decrease in the anodizing voltage at the end of TiO_2 Ntb film growth step-wise by δE_a = 0.5–1.0 V min^{-1}, intended for reducing the barrier layer thickness and it's resistance, was found also to be insufficient to achieve more uniform deposition from the tested acidic solution. Moreover, it was found that the tubular structure of TiO_2 Ntb films can be destroyed at the bottom of the tubes if anodizing voltage decrease is performed by larger δE_a steps. Surprisingly, when deposited under the same conditions from the same solution with pH = 5.3, adjusted by addition of TEA, the deposited species exhibit distinct morphologies and quite uniform dispersion along whole TiO_2 nanotube length even without decreasing the thickness of barrier layer (Fig. 12).

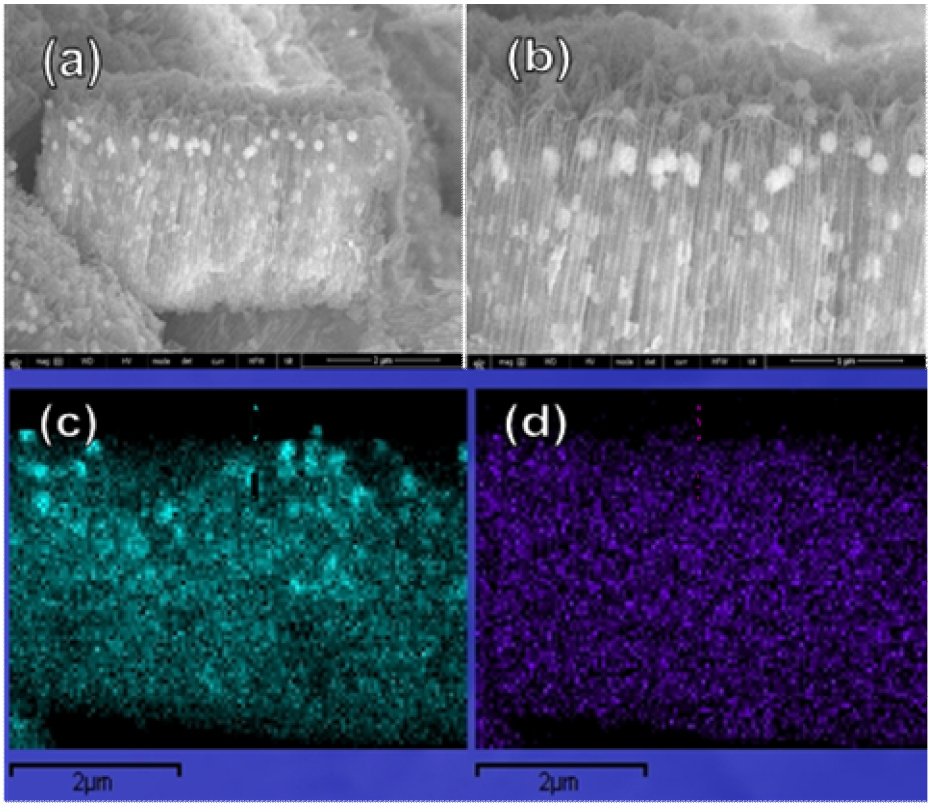

Fig. 12. (a, b) Cross-sectional FESEM images of TiO_2 Ntb film prepared and AC treated at $U_{p\text{-}to\text{-}p}$ = 1.2 V for 5 min in the same solutions as in Figure 1 adjusted to pH = 5.3; (c) and (d) show the 2D X-ray compositional maps of Cu and Se atoms, respectively, across the TiO_2 Ntb film.

In this case, the numerous round-shaped species were loaded quite uniformly throughout the whole thickness of TiO_2 Ntb film. The size of species encased inside the

film was found to be dependent on the AC treatment conditions attaining the diameter close to or even larger than the inner diameter of TiO_2 nanotubes.

The phase structure and composition of the products deposited inside the TiO_2 Ntb by AC treatment were further examined by X-ray diffraction. Figure 13 shows the typical patterns taken at a glancing angle from the TiO_2 Ntb films AC-treated in the both tested solutions, e.g., with pH 1.25 and pH 5.3. Note that in the former case (Fig. 13a), the peaks at 2h positions 29.76°; 39.98°; 49.76° and 51.46° should be, respectively, attributed to crystalline planes (111); (220); (311) and (202) of umangite, Cu_3Se_2, (tetragonal, space group P-421 m) according to PDF Card No. 04-003-6622, whereas the second group of peaks at 2h positions 22.88°; 44.56° and 65.16° belongs to cubic berzelianite, Cu_2Se, planes (111), (220) and (400) in accordance with DB card No. 04-006-1705.

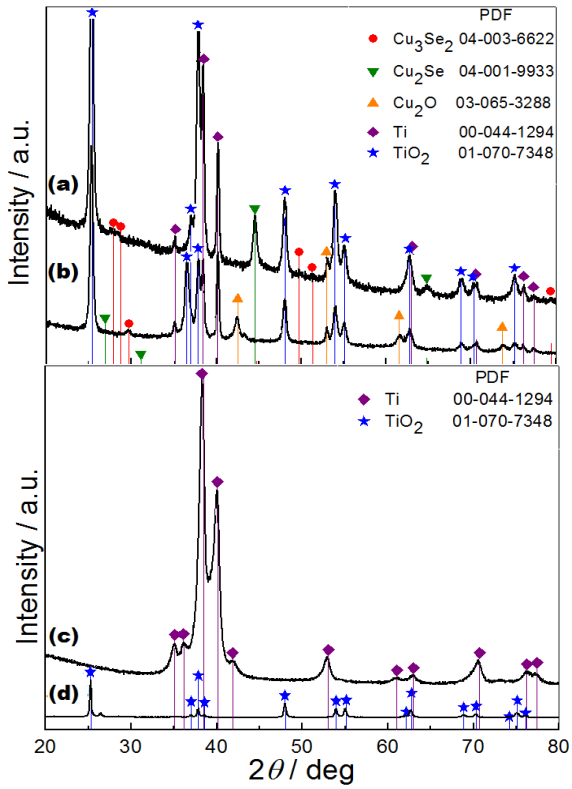

Fig. 13. Glancing angle XRD patterns of TiO_2 Ntb films fabricated as in Fig. 9 (a) and Fig. 10 (b). For comparison XRD patterns for a same pure TiO_2 Ntb film and Ti foil are shown in (c) and (d), respectively.

A remarkable fact is that the content of Cu_2Se crystallites was approximately three times higher than that of Cu_3Se_2. Note that according to XRD patterns taken at a glancing angle from Ti foil and annealed TiO_2 Ntb film (Fig. 13c and d), a set of well-

defined peaks at 2h positions 25.32°, 37.88°, 38.58°, 48.08°, 54.02°, 62.86° and 75.34° come from anatase TiO_2 planes (101), (004), (112), (200), (105), (116) and (215), respectively, whereas the peaks at 2h = 35.18°, 39.96° and 40.24° belong to the diffraction from the Ti planes (100), (002) and (101). None of the peaks could be indexed to Cu^0 or CuO.

The diffraction pattern of the TiO_2 Ntb film AC-treated in the same solution adjusted to pH 5.3 by the addition of TEA, however, differs significantly (Fig. 13b). In this case, besides the peaks marked with star, attributable to TiO_2 anatase, and those marked with cubes, ascribed to metallic Ti from the substrate (PDF card No. 00-044-1294), additional peaks at 2h positions 36.64°, 42.48°, 61.76° and 73.84° are observed. In accordance with PDF card No. 03-065-3288, these peaks can be indexed to cubic structure of Cu_2O. According to calculations using Scherrer formula, the average size of Cu_2O crystallites deposited inside the TiO_2 Ntb film under the same AC treatment conditions was 270 nm, which is thrice larger than the inner diameter of TiO_2 nanotubes implying on the destroy of titania nanotube walls at the deposition places by growing crystals. Furthermore, only traces of copper selenide were detected inside the TiO_2 Ntbs even after prolonged AC treatment in this solution. These data implied that decoration of TiO_2 nanotubes with pure copper selenides should be preferably performed in more acidic Cu(II)-H_2SeO_3 solutions.

In view of the aforementioned facts, several attempts were further made to increase the uniformity of TiO_2 Ntbs loading with copper selenide species from the Cu(II)-H_2SeO_3 solution with a pH 1.25. These attempts were mainly addressed to decrease the resistance of TiO_2 Ntb film by hydrogen insertion and titania doping before deposition. To the best of our knowledge, however, spillover hydrogen effect has never been used for more uniform electrochemical decoration of TiO_2 Ntb films with lower bandgap semiconducting nanospecies. It should be noted in this respect that, according to the literature, the resistance of TiO_2 crystallites as well as TiO_2 Ntb films can be reduced drastically by 8.6 orders down to ~ 10 X cm^{-2} due to spillover effect characteristic for TiO_2|Ti interfaces upon absorption of hydrogen. When investigating hydrogen doping on the uniformity of the TiO_2 nanotubes loading, as well as on the composition and phase purity of deposited copper selenide species, several pretreatments of TiO_2 Ntb before

depositions were examined. In this way, alternating current, 50 Hz frequency, as well as cathodic pretreatment in the acidic 0.005–0.05 mol L^{-1} H_2SeO_3 and 0.005–0.025 mol L^{-1} H_2SO_4 solutions under both DC and AC modes were tested. In addition, some deposition experiments were performed after keeping of working TiO_2 Ntb /Ti electrodes in hydrogen gas atmosphere at about 1.5 atm pressure and ambient temperature for 1 h.

3.2.2. Decoration of TiO_2 Ntb films with copper selenides after pretreatment in the acidic solutions

Concerning pretreatments in H_2SeO_3 solutions, there are few disappointing things. First of all, in these solutions under DC mode even at low potentials, ca. at -0.5 V, the deposition of selenium was observed. This effect was not apparently seen for AC treated films even up to $U_{p\text{-}to\text{-}p}$ = 1.2 V. However, in the case of AC pretreatment in 0.05 mol L-1 H_2SeO_3, obvious reconstruction of TiO_2 Ntb structure was revealed: nanotubes became brittle and crushed disorderly upon the specimen bending. This remarkable fact most likely could be ascribed to instability of anatase TiO_2 tubes in the acid solutions with molarities larger than 0.01 mol L^{-1}, as has been suggested recently. As regards AC pretreatment in more diluted H_2SeO_3 solution, e.g. 0.005 mol L^{-1}, this procedure was conducted at current densities of 5–7 mA cm^{-2} for 1 min, resulting in the bluish coloring of TiO_2 Ntb film without a significant damage of tubes structure. Note that bluish coloring of anatase TiO_2 should be ascribed to H^+ doping via reaction:

$$Ti^{4+}O_2 + H^+ + e^- \leftrightarrow Ti^{3+}O(OH) \quad (6)$$

In this case, the content of encased copper selenide species inside the hydrogen-sensitized TiO_2 Ntb film and uniformity of loading along the tubes by AC treatment in the deposition solution was found to be dependent on the AC pretreatment conditions in 0.005 mol L^{-1} H_2SeO_3 as well as on the TiNT film thickness. For thicker films, e.g., ≥ 10 μm, a significantly more species were deposited at the bottom of nanotubes than inside the film bulk, whereas in the case of thinner films, e.g., 4–5 μm, larger quantity of species was tethered to the TiO_2 Ntb walls inside the film bulk. Judging from the EDX analysis, Cu species are mainly composed of Cu_2Se.

FESEM, as well as EDX studies, confirmed that no deposition took place from the tested acidic Cu(II)-H_2SeO_3 solution inside the nanotubes of TiO_2 film hydrogen-doped

in H_2SO_4 solution by DC pretreatment at potentials as low as -0.5 V. Similar results were also obtained for TiO_2 Ntb films doped by AC pretreatment even in diluted H_2SO_4 solutions within 0.5 to 1.0 V $U_{p\text{-}to\text{-}p}$ range at current densities of ~ 6.0 to 50 mA cm^{-2} and the subsequent AC deposition in the tested solution at $U_{p\text{-}to\text{-}p}$ ranging between 0.7 and 1.3 V. In this case, only insignificant amount of copper and selenium containing species was deposited at the bottom of some nanotubes (Fig. 14b). This is opposite to what would be expected and probably could be linked with the significant TiO_2 Ntb structural reorganizations to nanoparticulate architecture taking place even during short time pretreatment in the sulfuric acid solution (Fig. 14a).

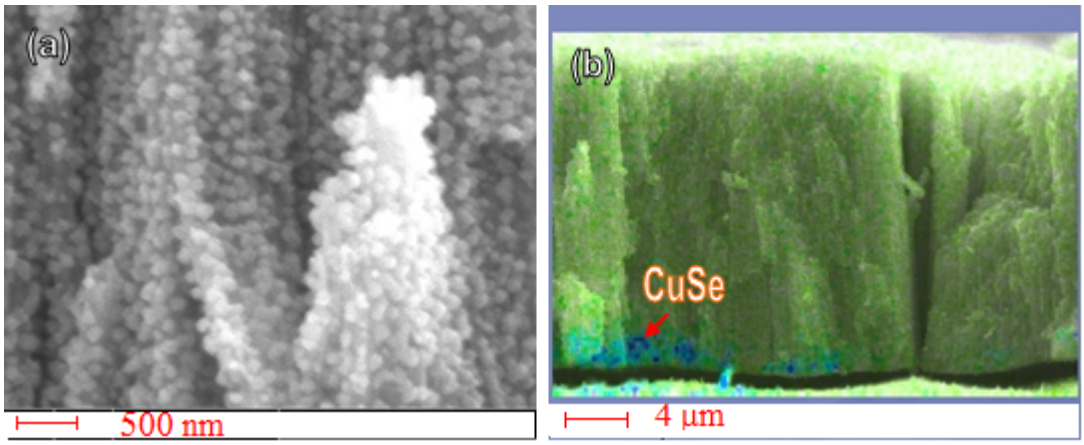

Fig. 14. Cross-sectional SEM (a) and X-ray mapping (b) images of TiO_2 Ntb film grown by Ti anodizing in Etg electrolyte at 50 V for 30 min, then annealed at 450 °C for 2 h and AC treated in 0.05 mol L^{-1} H_2SO_4 (a) or 0.005 mol L^{-1} H_2SO_4 (b) at $U_{p\text{-}to\text{-}p}$ 0.5 V for 60 s and, finally, in Cu(II)-H_2SeO_3 (pH=1.3) solution at $U_{p\text{-}to\text{-}p}$ 1.3 V for 10 min.

3.2.3. Sensitization of TiO_2 Ntb in an alkaline solution

A significantly larger content of copper selenide was deposited inside the TiO_2 Ntbs after film doping in an alkaline 0.5 mol L^{-1} KOH solution by AC pretreatment at $U_{p\text{-}to\text{-}p}$ 1.0 to 1.3 V for 1.0 min. Figure 15 depicts the SEM maps of TiO_2 Ntb film grown at 50 V for 20 min (a,d) and the distribution profiles of Cu and Se elements, composing deposited species, inside the TiO_2 Ntbs after hydrogen doping by AC pretreatment in the KOH solution and the subsequent depositions at $U_{p\text{-}to\text{-}p}$ = 1.2 (b, c) and 1.4 V (e, f). Evidently, in the both cases, copper selenide is deposited inside the film bulk differently, although any depositions at the film surface, characteristic for undoped film (Fig. 11), are seen. However, from the SEM observation and the elements map, the uniformity of depositions inside the treatment in the acidic Cu(II)-H_2SeO_3 solution can be ascribed to

tetragonal Cu_3Se_2 (space group P-421 m; PDF No 04-003-6622). The average size of these crystallites after deposition at $U_{p\text{-}to\text{-}p}$ = 1.3 V for 5 min is approximated to 33 nm.

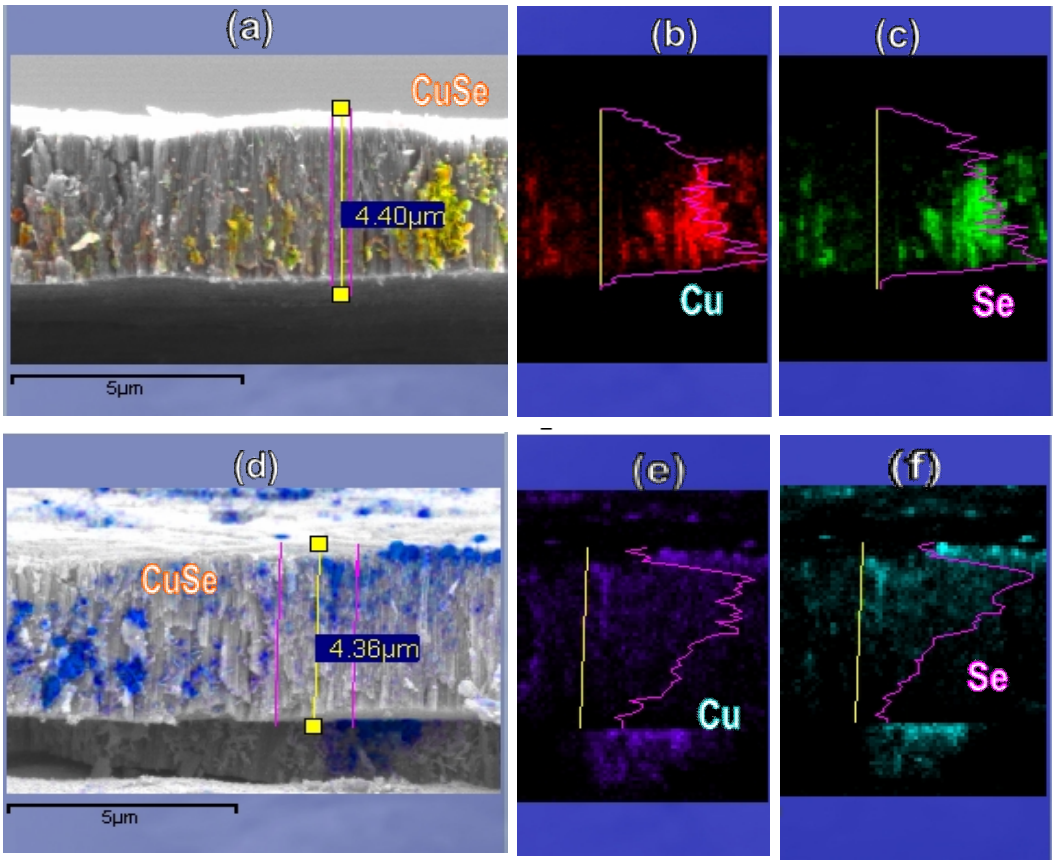

Fig. 15. Cross-sectional SEM view of Cu_xSe-in-TiO_2 Ntb film (a,d) and X-ray mapping of Cu (b,e) and Se (c,f) elements encased inside this film by AC deposition in the same as in Figure 11 solution at $U_{p\text{-}to\text{-}p}$ = 1.2 V (a-c) or $U_{p\text{-}to\text{-}p}$ = 1.4 V (d-f) for 5 min. Before deposition, film was doped with hydrogen in 0.5 M KOH solution at AC $U_{p\text{-}to\text{-}p}$ = 1.2 V for 1 min.

3.2.4. Decoration of TiO_2 Ntb films after keeping in the hydrogen atmosphere

To investigate the influence of H_2 doping, Ti specimens anodized at 50 V after annealing were kept in the H_2 atmosphere at 1.5 atm pressure and ambient temperature for 60 min, and then AC treated in the deposition solution and characterized. Figure 16 shows the typical FESEM images and distribution profiles of Cu and Se elements across the TiO_2 Ntb film for specimens H_2 doped and AC treated in the deposition solution. In this case, quite uniform loading of copper selenide species onto the nanotube walls can be seen at the middle of the film in thickness of ~4.0 μm (Fig. 16a). For the thicker TiO_2 Ntb films, ca. 10 μm, a significantly larger quantity of species was deposited at the bottom of the film (Fig. 16c, d).

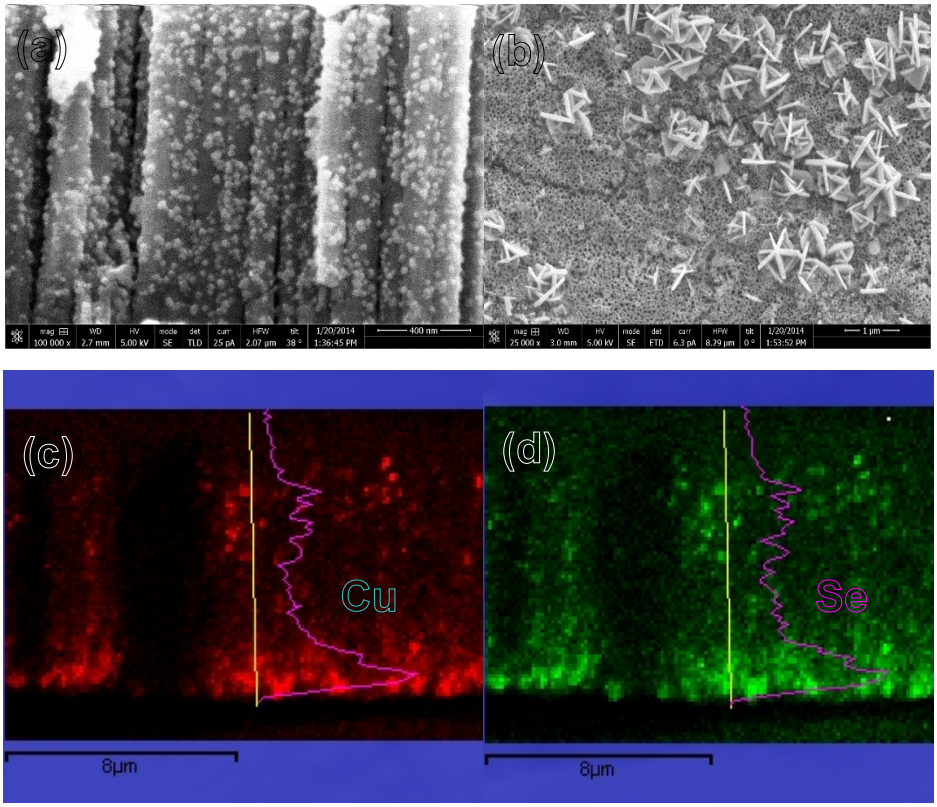

Fig. 16. Cross-sectional (a) and top-side (b) SEM images and X-ray mapping of Cu (c) and Se (d) elements encased inside the TiO_2 Ntb film by AC deposition in the same solution as in Figure 11 at $U_{p\text{-}to\text{-}p}$ = 1.1 V for 5 min. TiO_2 Ntb film was grown at 50 V for 1 h, annealed and treated in H_2 atmosphere for 1 h.

It is noteworthy, that under these conditions, some quantity of weakly attached, rod-shaped crystallites of up to 0.7 μm in length was also formed on the film surface (Fig. 16b) which can simply be removed by ultrasound agitation. Figure 17b shows the typical XRD pattern taken at a glancing angle from the TiO_2 Ntb film AC treated in the acidic Cu(II)-H_2SeO_3 solution (pH 1.25) after the specimen doping in H_2 atmosphere.

In the present case, in accordance with PDF Card No. 04-0107893, the peaks at 2Θ positions 26.58°, 28.10°, 31.20°, and 45.54° should be attributed, respectively, to crystalline planes (311), (312), (006), and (317) of copper selenide, CuSe, (hexagonal, space group P-P63/m). Note that except the diffraction peaks of CuSe, anatase TiO_2, and Ti, marked, respectively, by cubes, stars, and points, additional peaks at 2Θ positions 26.58°, 44.54°, and 64.9° are seen. According to PDF card No 04-004-4729, these peaks are associated with the presence of $Cu_{1.8}Se$ (berzelianite). The average size of deposited crystallites, calculated by Scherrer approach, was approximately equal to 88 nm.

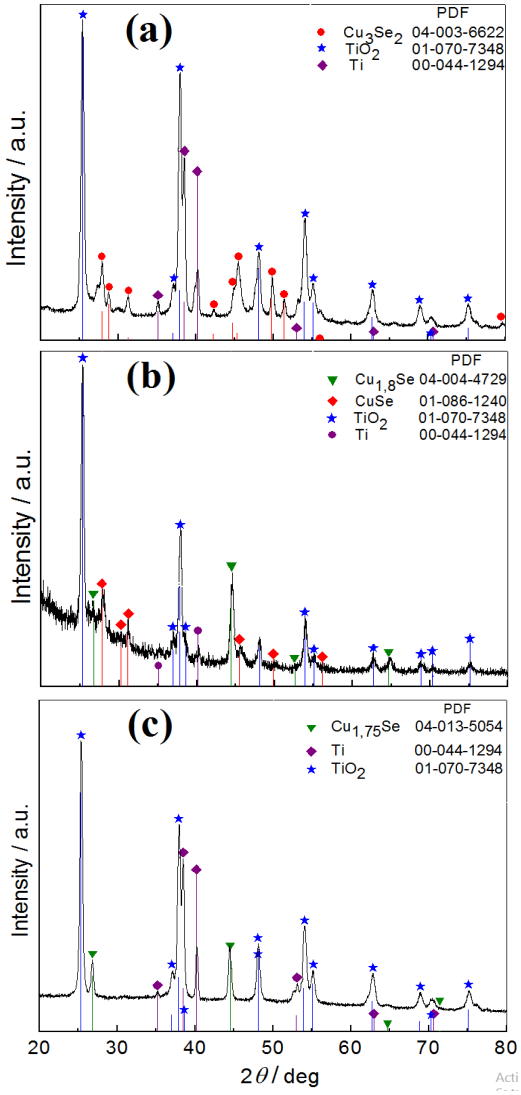

Fig. 17. XRD patterns of TiO_2 Ntb films decorated with copper selenide species by AC treatment in the solution as in Figure 11 at $U_{p\text{-}to\text{-}p}$ = 1.3 V for 5 min. Before depositions, TiO_2 Ntb films were sensitized in 0.5 mol L^{-1} KOH solution by AC treatment at $U_{p\text{-}to\text{-}p}$ 1.2 V for 1.0 min (a,c) or holding in H_2 atmosphere for 1 h (b). In (c): XRD pattern of a same TiO_2 Ntb/Cu_2Se_3 heterostructure as in (a) after annealing at 300 ºC for 2 h.

3.2.5. Annealing effect of TiO_2 Ntb film decorated with copper selenides

According to the results obtained investigating the annealing effects on copper selenides encased in alumina matrix, the annealing at 300 °C results in the formation of superionic conductor $Cu_{2-x}Se$ species. In the present research, similar results were obtained for copper selenides encased inside the TiO_2 nanotubes. For example, Figure 18c depicts the typical pattern of TiO_2 Ntb/Cu_3Se_2 heterostructure after annealing at 300 °C for 2 h. In this case, the comparison of the observed peaks at 2Θ positions 26.76°, 44.46°, 53.1°, and 65.23° with the standard PDF cards showed that after

annealing the species encased in TiO_2 Ntb film possessed crystalline structure matching well with a cubic $Cu_{2-x}Se$ with x = 0.25 (space group Fm-3 m, PDF Card No 04-0135054). We expect that tethering of super ionic conductor species, particularly $Cu_{1.75}Se$, capable of absorbing visible as well as near IR light, due to direct bandgap E_g = 2.1–2.3 eV and indirect E_g = 1.2–1.4 eV, should widen drastically the absorption region by this heterostructure.

3.2.6. Optical properties

The optical properties of TiO_2 Ntb films decorated with various copper selenide species were studied by means of analyzing their diffused reflectance spectra using the Kubelka–Munk function: [$K = (1-R_d)^2/2R_d$], hereafter Tauc plot was applied for determination of heterostructure band gaps for allowed direct and indirect transitions. Figure 18 illustrates typical Tauc plots calculated from the experimental diffuse reflectance and absorption spectra versus photon energy for the bare TiO_2 Ntb and TiO_2 Ntb/Cu_3Se_2 heterostructured films. Note that bare TiO_2 Ntb film demonstrated significantly higher reflections within the 350 to 500 nm light range than the same film decorated with copper selenide species. Moreover, analysis of corresponding absorption plots for possible allowed direct transitions shows that except the absorption edge typical for annealed and H^+-doped bare TiO_2 Ntb film (~3.39 eV), an additional absorption edge in the visible region appeared for Cu_3Se_2-in-TiO_2 Ntb samples (Fig. 18). The new absorption edge into the visible light region was found to be dependent on the content of tethered selenide species. For TiO_2 Ntb films with nonclogged tubes, E_g shifted down to ~2.0 eV (Fig. 18c) and likely should be linked with optical properties of semiconducting copper selenide. It should be pointed out that the same effect was also seen for the higher energy sub-bands in UV region where E_g = 3.39 eV for bare TiO_2 Ntb film was shifted to E_g = 3.31 eV and E_g = 3.16 eV after AC depositions of Cu_3Se_2, which lasted 60 and 120 s, respectively. In contrast, this effect was not observed for TiO_2 Ntb films evidently covered by Cu_3Se_2 crystallites (not shown herein), thus forming the absorption edge in the IR region (E_g = 1.12 eV), which is near the optimum value for Solar cell applications.

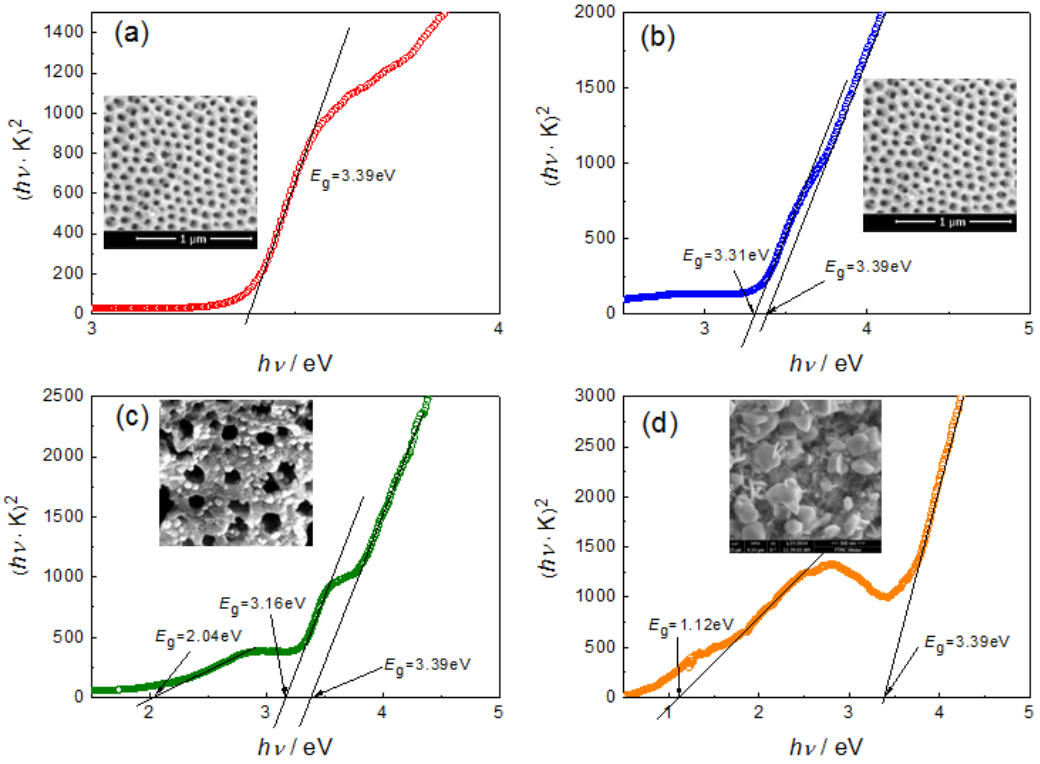

Fig. 18. Tauc plots calculated from the experimental diffuse reflectance spectra for allowed direct transitions in the bare TiO_2 Ntb film (a) and the same film decorated by electrodeposition from the same solution as in Figure 11 at $U_{p\text{-}to\text{-}p}$ = 1.3 V for 1.0 (b), 2.0 (c) and 7.0 min (d). To achieve loading of copper selenide species mainly onto the Ntb walls, all specimens before deposition were subjected to AC pretreatment in 0.5 mol L^{-1} KOH solution at $U_{p\text{-}to\text{-}p}$ = 1.2 V for 60 s. Insets depict the top-side SEM images of heterostructured films.

Discussion

The idea of titania nanotubed films doping with hydrogen for more uniform electrochemical deposition of copper selenide nanospecies aroused from the numerous indications on the significant resistance decrease of titania materials contacting with the metal capable sorb atomic as well as molecular hydrogen at room temperature. Electrical conductivity increase due to the interaction of hydrogen with TiO_2 tethered to metal has been reported in several works implying on the electron transfer from atomic hydrogen species to the metal oxide. To the best of our knowledge, variation in the electrical resistance of Ti/TiO_2 Ntb electrodes upon expose in hydrogen atmosphere or hydrogen electroreduction has not been reported yet. However, voltage-current (*E*-*I*) plots of Ti/TiO_2 Ntb and Ti/TiO_2Ntb-Cu_xSe specimens, fabricated under conditions of this study, revealed large differences between these two samples (Fig. 19). Particularly, the

resistance of crystalline TiO_2 Ntb film, which was formed at 30 V for 120 min and calcined at 450 °C (~ 38 GΩ), decreased down to ~ 20 kΩ, i.e. by 6 orders of magnitude, after treatment in the H_2 atmosphere at ~ 1.5 atm and room temperature for 1 h. Therefore, under conditions of hydrogen evolution reaction in the tested aqueous solutions, the resistance of Ti/TiO_2 Ntb electrode can attain the level of hundred ohms, thus providing the basis for titania tubes uniform decoration by electrochemical approach.

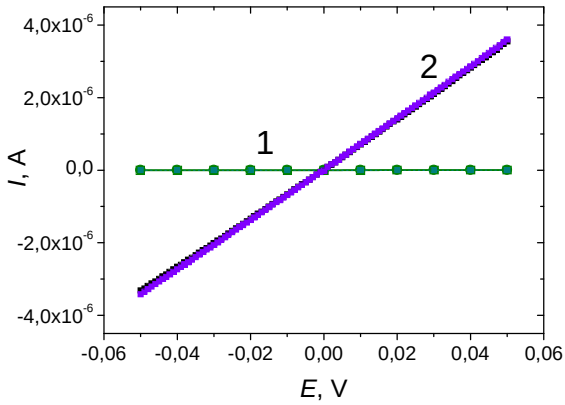

Fig. 19. Typical variations of the current strength on the potential applied for the TiO2 Ntb film grown by Ti anodizing at 30 V for 2 h and annealed at 450 ºC for 2 h before (1) and after (2) exposition in H_2 atmosphere at 1.5 atm pressure for 1 h.

The physical nature of the hydrogen spilt-over species capable adsorb in the metal, such as Pd, Pt, Rh, Ru, Ti and Mo side and diffuse to contacting metal oxide phase, such as TiO_2, WO_3, V_2O_5 and MoO_2, has been a subject of numerous investigations in the past decades. Atomic, ionic, radical and bound hydrogen species have been considered in the literature as spilt-over. The recent models proposed to explain the resistance decrease of metal oxides attached to the metal capable adsorb hydrogen are based on the description of absorbed hydrogen as electron donor via recombinative desorption. A more detailed description of the adsorbate – support interaction can be explained in terms of the Wolkenstein model of chemisorption.

3.3. Decoration of TiO_2 nanotube films with nanoplatelet MoS_2

3.3.1. Hydrothermal synthesis of crystalline MoS_2 nanoflowers

It has been recently reported that throughout the hydrothermal treatment of solution containing 15 mmol L^{-1} $(NH_4)_6Mo_7O_{24}$ + 270 mmol L^{-1} thiourea at 180 ºC "superaerophobic" MoS_2 film can be formed on the well cleaned surface of pure titanium sheet. Our investigations have indicated that such treatment leads also to the formation of black-colored powdered species in the solution bulk. According to XRD patterns, the crystallinity of these species is poor but increases with increase in the autoclaving temperature (Figure 20A). The main diffraction peaks of the product obtained at 225 °C are seen at 2theta 14.10, 32.89, 33.68, 39.50 and 58.73°.

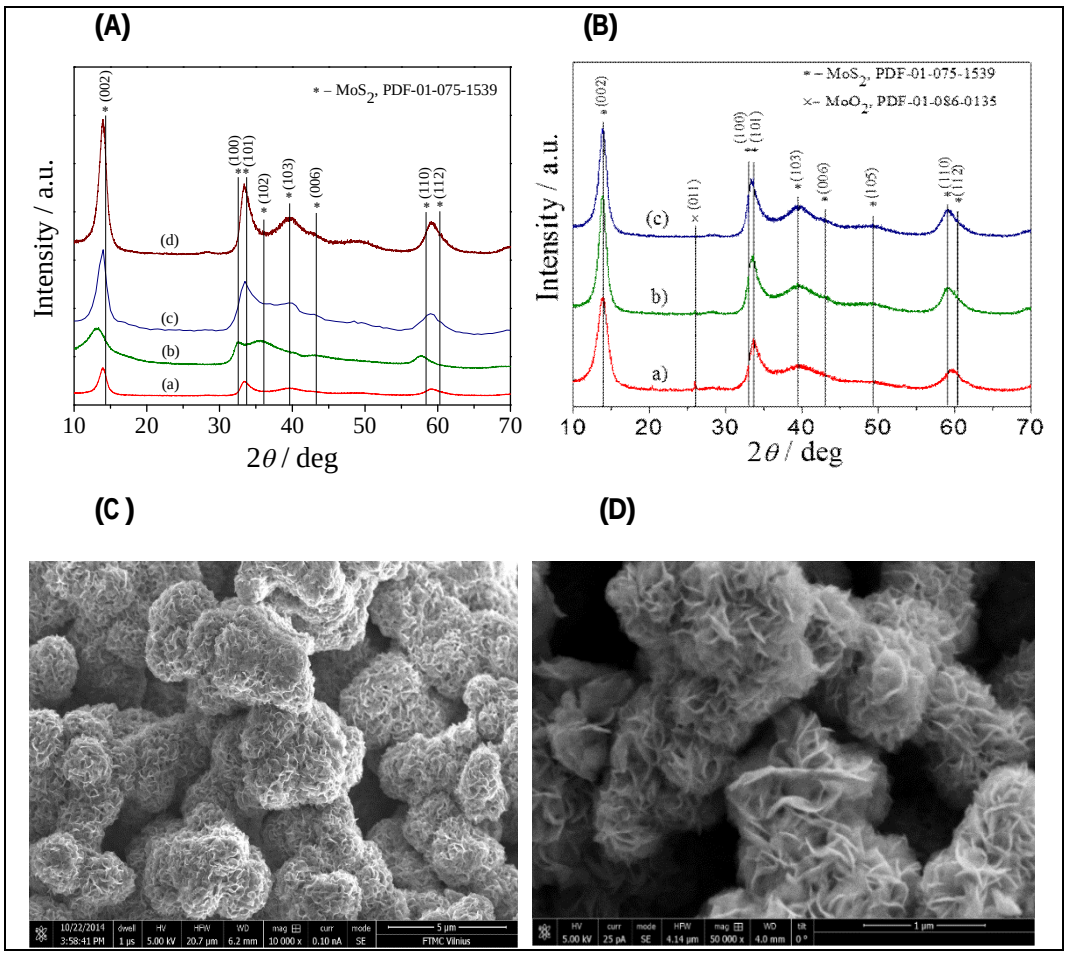

Fig. 20. XRD patterns of: (A) the products synthesized hydrothermally in an aqueous solution containing 15 mmol L^{-1} $(NH_4)_2Mo_7O_{24}$ + 270 mmol L^{-1} thiourea at 180º (a), 195º (b), 210º (c) and 225 ºC (d) for 20 hours; (B) the same for products synthesized at 195º (a), 210º (b), and 225ºC (c) for 20 h with (a,b) and without (c) subsequent calcination in oxygen-free atmosphere at 300ºC for 20 h. SEM images (C and D) demonstrate typical morphology of products synthesized hydrothermally at 225 °C for 20 h at different magnification.

According to PDF card no 01-075-1539, they match well with (002), (100), (101), (103) and (110) planes attributable to MoS_2, whereas decrease in the synthesis temperature below 220 °C results in the shift of the main diffraction peaks from the typical positions, pointing to the formation of more non-stoichiometric MoS_2.

We note that stoichiometry of these products can be significantly improved by prolonged annealing of these species at 300 °C in air (Figure 22). However, judging from the appearance of small diffraction peak at 2*theta* 26°, the annealing in air resulted in the formation of insignificant content of MoO_2 besides crystalline MoS_2, which was not formed by hydrothermal synthesis at 225 °C without the subsequent calcination (Fig. 20B).

As can be judged from the SEM images, the morphology of the products obtained in the tested solutions within the autoclaving temperature (T_a) range from 180 to 225 °C is quite similar, varying mainly in the size of agglomerated flower-type buttons (Figs 20 C and D). Note that increase in the T_a resulted in the formation of slightly larger MoS_2 buttons. To elucidate the nature of the synthesized MoS_2 products, their layer-dependent Raman spectra phonon modes were further studied in detail under 532 and 638 nm light excitation. Figure 21 demonstrates the effect of laser power on the Raman spectra of the products formed at 225 °C for 20 h. As seen, at relatively low laser powers (0.06-0.6 mW), the pair of bands at 408 and 382 cm^{-1} dominate in the Raman spectrum. Bulk MoS_2 excited with 532 nm laser line exhibits A1g (408 cm^{-1}) and E12g (383 cm^{-1}) Raman modes due to out-of-plane vibrations of only S atoms and opposite vibration of two S atoms with regard to Mo atom, respectively.

Thus, the observed spectra of this sample evidence the presence of 2-D layered MoS_2 having a 1.0 cm^{-1} lower separation value between A_{1g} and E^1_{2g} active modes. It is also seen that at excitation with higher laser power (3 mW), drastic changes take place in the spectrum, indicating decomposition of MoS_2, since the clearly defined peaks at 127, 151, 285, 337, 662, 819, and 993 cm^{-1} belong to orthorhombic α-MoO_3. To avoid chemical transformation of MoS_2, further experiments were conducted with 0.3 mW laser power.

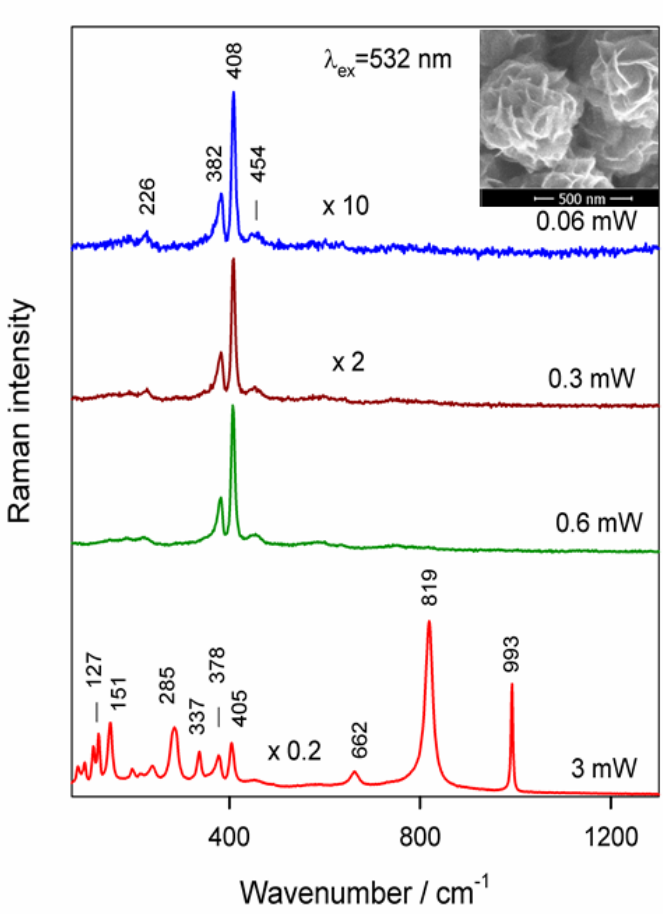

Fig. 21. Raman spectra of the product produced by autoclaving the solution as in Figure 20 at 225 ºC for 20 h and collected at different excitation laser powers. Excitation wavelength was 532 nm. The integration time was 300 s for 0.06 mW laser power and 100 s for other experiments. Inset: SEM image of the product.

3.3.2.Decoration of TiO_2 Ntb films with MoS_2

Further we investigated the possibility to decorate the surface of TiO_2 Ntbs with MoS_2 nm-sized species. Therefore, hydrothermal syntheses were carried out by inserting the Ti specimen covered with nanotubed titania film. Figure 22 shows typical SEM images of TiO_2 Ntb films before (A,B) and after hydrothermal treatment in the $(NH_4)_2Mo_7O_{24}$ and thiourea solutions illustrating different loadings with MoS_2. In the case of the most concentrated solution tested herein, namely, the one comprised of 15 mmol L^{-1} $(NH_4)_2Mo_7O_{24}$ and 270 mmol L^{-1} thiourea, the TiO_2 Ntb film surface was completely covered with MoS_2. Moreover, it seems likely that some nanotubes at the surface side were clogged as well (not shown herein). In contrast, nice decoration of titania tubes with nanoplatelet species having abundance of exposed edges was obtained in the diluted solutions composed of only 1 to 3 mmol L^{-1} $(NH_4)_2Mo_7O_{24}$ and 18 to

54 mmol L^{-1} thiourea with all other conditions being the same (Figures 22 C-F). It is noteworthy that only in the diluted solutions uniform covering of nanotubes along their whole length was obtained (Fig. 22F) pointing to the affinity between the fabricated nano platelets and the titania surface. At the same time significantly smaller and less agglomerated spherical particles resembling cabbages composed of numerous leafs with exposed edges were fabricated in the solution bulk. It was found also that the average size of 2-D platelet species can be controlled by varying the solution concentration. In the case of 3.0 mmol L^{-1} heptamolybdate and 54.0 mmol L^{-1} thiourea, the autoclaving at 225 °C for 20 hours yielded tethered nanoplatelets with average length of less than 100 nm and a few nanometer thickness at their edges.

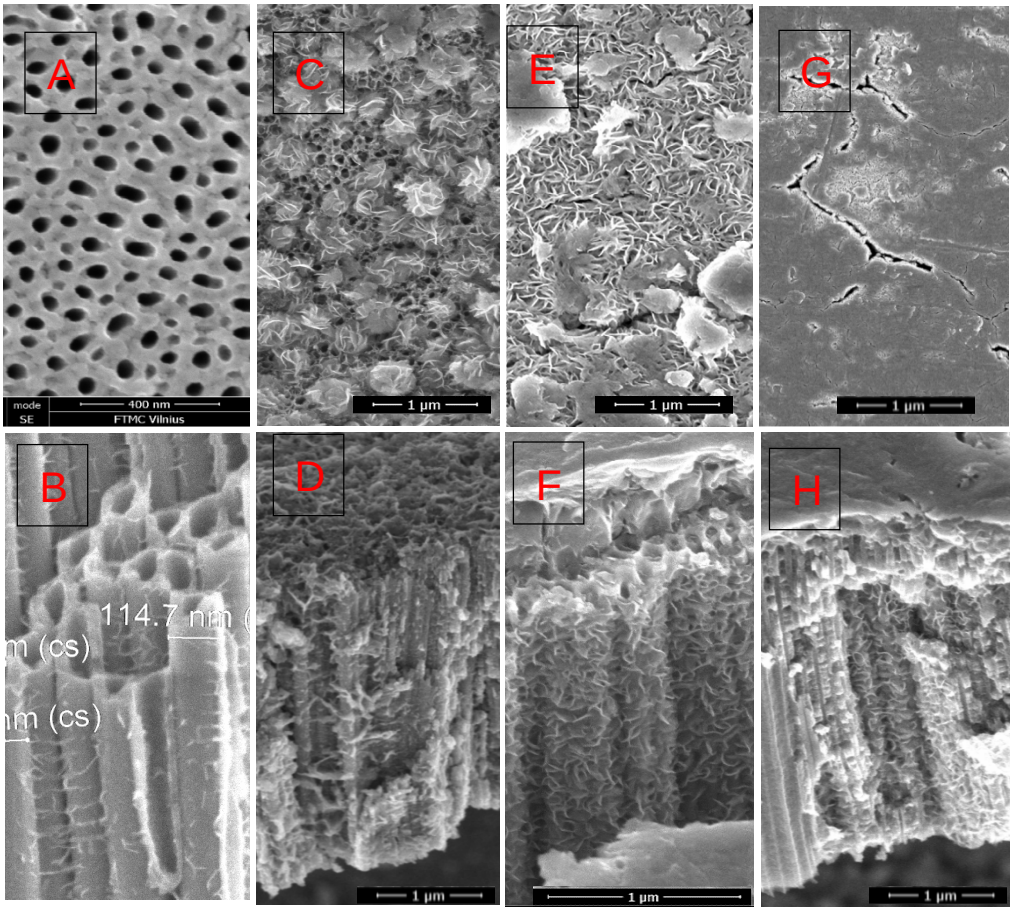

Fig. 22. Characteristic FESEM views of TiO_2 Ntb films before (A,B) and after (C-H) hydrothermal treatment at 225 ºC for 20 hours in the solutions containing $(NH_4)_2Mo_7O_{24}$ + $CS(NH_2)_2$ (in mmol L^{-1}): 1.0 + 18.0 (C,D); 3.0 + 54 (E,F); 15.0 + 270 (G,H).

3.3.3. Voltammetric measurements.

Photo-sensitivity of Ti electrodes covered with nanotubed anatase-TiO_2 film and heterostructured with MoS_2 2-D species was investigated in the solution of 0.1 mol L^{-1}

KOH via determination the variation of the open-circuit potential (E_{oc}) under simulated solar light illumination. The results obtained for TiO_2 Ntb film before and after MoS_2 loading are shown in Figure 23A. One can see that both pure TiO_2 Ntb and TiO_2 Ntb decorated with MoS_2 species demonstrate typical behavior of n-type semiconductors. In the case of calcined TiO_2 Ntb film, E_{oc} values under illumination and in dark lie within the range of TiO_2 according to Pourbaix diagram and the magnitude of ΔE_{oc} between the values in dark and light is about 250 mV. The magnitudes of E_{oc} and ΔE_{oc} of TiO_2 Ntb-MoS_2 heterostructured electrodes depend significantly on the content of MoS_2 deposited onto the TiNT film surface. In the case of complete coverage with bulk MoS_2, characteristic for concentrated solutions, electrodes became non photosensitive, whereas moderate decoration of film with MoS_2 species resulted in the increase of E_{oc} value seen at the illumination period.

Cyclic voltammetry (CV) was applied further in an acidic solution of 0.5 mol L^{-1} H_2SO_4 to investigate the catalytic performance of bare and MoS_2-decorated TiO_2 films. For comparison, Pt electrode was also tested. As seen (Fig. 23B, curve 1), the capability of Ti electrode covered with nanotube-shaped anatase-TiO_2 film of ~ 4.1 μm thickness with average tube diameter of ~ 110 nm, to generate hydrogen gas is very poor even at -0.5 V versus RHE.

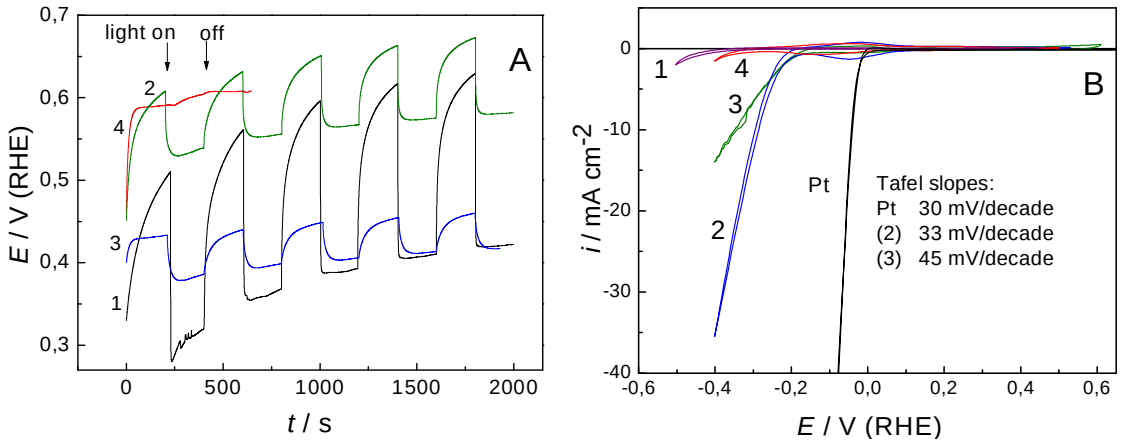

Fig. 23. (A) Variation of the open-circuit potential of Ti/TiO_2 Ntb electrode upon illumination in 0.1 mol L^{-1} NaOH solution before (1) and after (2-4) decoration with MoS_2 nanoplatelet species by hydrothermal treatment in the solutions containing $(NH_4)_2Mo_7O_{24}$ + $CS(NH_2)_2$ (in mmol L^{-1}): (2) 1 + 18, (3) 3 + 54 and (4) 15 + 270 at 225 °C for 20 h. (B): Cyclic voltammograms for Pt and the same electrodes as in (A) in deaerated 0.5 mol L^{-1} H_2SO_4 solution, potential scan rate 5 mV s^{-1}; the corresponding Tafel plots are presented in the Inset.

The performance of the same electrode decorated with MoS_2 in electrocatalytic generation of hydrogen was found to be strongly dependent on the concentration of heptamolybdate / thiourea solution used for hydrothermal treatment of TiO_2 Ntb film with all other conditions being the same (see plots 2 to 4 in Fig. 23B).

It is worth noticing that the performance of Ti/TiO_2 Ntb/MoS_2 electrodes decorated in the concentrated solution (curve 4) remained quite low and similar to that of bare TiO_2 Ntb film. However, Ti/TiO_2 Ntb electrodes which underwent hydrothermal treatment in the solution containing only 1.0 to 3.0 mmol L^{-1} ammonium heptamolybdate and 18 to 54 mmol L^{-1} thiourea at 220-225 °C exhibited nice catalytic performance for hydrogen evolution reaction. The stability of catalytic performance of Ti/TiO_2 Ntb-MoS_2 electrodes was further investigated in the 0.1 mol L^{-1} H_2SO_4 solution by potential cycling within 0.04 V to -0.4 V at 10 mV s^{-1} potential sweep rate.

Discussion

In summary, we present herein for the first time a facile and efficient strategy for decoration of titania nanotubed films with crystalline nanoflowered and nanoplatelet MoS_2 species using modified one step hydrothermal method. By this strategy, TiO_2 Ntb films heterostructured with nanoplatelet MoS_2 species, densely packed along the whole nanotube length, were formed at 210 - 225 °C in the solutions containing only 0.5 to 3.0 mmol L^{-1} of ammonium heptamolybdate and 9 to 54 mmol L^{-1} of thiourea. Use of diluted solutions prevents clogging of the tubes and complete blocking of the TiNT film surface. It is also shown, that MoS_2-decorated TiO_2 Ntb films demonstrate good electrocatalytic activity in hydrogen evolution reaction taking place in acidic solution with the Tafel slopes of 32-37 mV per decade.

4. CONCLUSIONS

1. The methods for uniform decoration of anatase TiO_2 nanotube (Ntb) films with Cu_2O nanoparticles were proposed: with weakly acidic copper acetate electrolyte and alternating current. Growth of pure Cu_2O crystals in the TiO_2 Ntbs was based on thermodynamic analysis of the solution.

2. It has been discovered that TiO_2 Ntb films decorated with Cu_2O nanoparticles are able to absorb not only the UV light, but visible light as well. By increasing amount of Cu_2O deposited in the TiO_2 nanotubes, the TiO_2 Ntb – Cu_2O absorption edge can be moved up to 2.1 eV.

3. The possibility of electrochemical decoration of TiO_2 Ntb film with semiconducting copper selenide nanoparticles in aqueous solutions and the peculiarities of the process were investigated. The effect of hydrogen doping of the Ti/TiO_2 Ntb electrode for uniform decoration of TiO_2 nanotubes with semiconducting nanoparticles was used for the first time.

4. It was determined that TiO_2 Ntb – Cu_2O heterostructures are characterised by significantly lower dependence on the angle of incidence of excitation beam – this can be especially useful for solar cell circuits.

5. Investigated optical properties and light absorption features of TiO_2 Ntb decorated with copper selenide (Cu_3Se_2 and $Cu_{2-x}Se$) nanoparticles.

6. Optimized composition of hydrothermal processing solution and conditions for decoration of TiO_2 Ntb film surfaces and nanotubes with nanoleafed MoS_2 . The uniform formation of crystalline MoS_2 on the TiO_2 surface is achieved with low concentration ammonium heptamolybdate and urea solutions within the temperature of 220 to 225 °C.

7. It was determined that Ti/TiO_2 Ntb – MoS_2 electrodes catalyse hydrogen release from acidic solutions and the reaction is characterized by stability.

List of Publications

ISI Referred Journals

1. A. Jagminas, **J. Kovger**, G. Niaura, J. Juodkazytė, A. Selskis, R. Kondrotas, B. Šebeka, J. Vaičiūnienė, A. Rėza. *"Decoration of the TiO_2 nanotube arrays with copper suboxide by AC treatment"*. Electrochim. Acta 125 (2014) 516 – 523.

2. J. Juodkazytė, B. Šebeka, I. Savickaja, A. Jagminas, V. Jasulaitienė, A. Selskis, **J. Kovger** and P. Mack. "*Study on copper oxide stability in photoelectrochemical cell composed of nanostructured TiO_2 and Cu_xO electrodes"*. Electrochim. Acta 137 (2014) 363 – 371.

3. A. Jagminas, **J. Kovger**, A. Selskis, A. Rėza. *"Effect of hydrogen doping on the loading of titania nanotube films with copper selenide species via alternating current deposition"*. J. Appl. Electrochem. 45 (2015) 1141–1151.

Other Referred International Journals

4. R. Žalnėravičius, A. Paškevičius, **J. Kovger**, A. Jagminas. "*Fabrication by AC Deposition and Antimicrobial Properties of Pyramidal-Shaped Cu_2O-TiO_2 Heterostructures"*. Nanomaterials and Nanotechnology 4 (2014) 31 (1 – 8).

5. **J. Kovger**, A. Naujokaitis, G. Niaura, J. Juodkazytė, G. Valušis, A. Jagminas. *"Research on hydrothermal decoration of TiO_2 nanotube films with nanoplatelet MoS_2 species"*. Nanomaterials and Nanotechnology 6 (2016) 1-9.

Conference Materials

1. A. Jagminas, **J. Kovger**, G. Niaura, J. Vaičiūnienė. *"Alternating current deposition of semiconducting particles as a new prospective approach for controlled functionalization of TiO_2 nanotubed films"*. "CHEMIJA 2013" 11-oji lietuvos chemikų tarptautinė konferencija P.23. (2013) Vilnus, Lithuania.

2. A. Jagminas, **J. Kovger**, A. Rėza. *"Decoration of the TiO_2 nanotube films by AC treatment for enhanced photoresponse"*. Proceedings of EMN Spring 2014 Meeting, pp. 201 – 202. (2014) Las Vegas, JAV (oral).

3. **J. Kovger**. *"TiO_2 nanovamzdelinių plėvelių elektrocheminio dekoravimo vario junginių nanodariniais tyrimas"*. Doktorantų ir jaunųjų mokslininkų konferencija". (2014) Vilnius, Lithuania (oral).

4. **J. Kovger**, R. Karpič, I. Vrublesky, K. Chernyakova, A. Jagminas. *"Effect of Low-Energy Oxygen Plasma Treatment on Photoluminescence of Carbon-Bearing Porous Alumina"*. Conference "Interaction of Radiation with Solids". (2015) Minsk, Belarus.

TITANO ANODINIŲ PLĖVELIŲ DEKORAVIMO MATOMĄ ŠVIESĄ SUGERIANČIAIS PUSLAIDININKIŲ NANODARINIAIS TYRIMAS

Reziumė

Naujų nanostruktūrizuotų medžiagų, jų tvarkių kolonijų, sluoksniuotų plėvelių bei heterostruktūrų sintezė ir konstravimas šių dienų mokslininkams leidžia sukurti naujų ar geresnių savybių medžiagas, nulemsiančias ateities mokslo ir technologijų pažangą.

Disertacinis darbas siejasi su perspektyviais, nanostruktūrizuotų TiO_2 sluoksnių ir plėvelių kompozitų su kitų puslaidininkių nanodalelėmis tyrimais, grindžiamais jų nekenksmingumu aplinkai, pigumu, cheminiu ir mechaniniu atsparumu.

Šio darbo tikslas buvo ištirti anodinės TiO_2 plėvelės nanovamzdelių elektrocheminio dekoravimo žemesnės draustinės juostos puslaidininkių nanodalelėmis galimybes. Darbo metu buvo pasiūlytas silpnai rūgštus vario acetato elektrolitas ir tinklo dažnio kintamosios srovės metodas anatazo TiO_2 nanovamzdelinių (Nv) plėvelių tolygiam dekoravimui CuO_2 nanodalelėmis. Parodyta, kad Cu_2O nanodalelėmis dekoruotos TiO_2 Nv plėvelės geba absorbuoti ne tik UV, bet ir regimąją šviesą. Didinant TiO_2 nanovamzdeliuose nusodinto ant jų sienelių Cu_2O, TiO_2 Nv – Cu_2O absorbcijos kraštą galima pastumti iki 2,1 eV. Ištirtos taip pat TiO_2 Nv plėvelių elektrocheminio dekoravimo puslaidininkinėmis vario selenidų nanodalelėmis galimybės vandeniniuose tirpaluose bei proceso ypatumai. Tolygiam nanovamzdelių dekoravimui šių puslaidininkių- nanodalelėmis pirmą kartą panaudotas Ti/TiO_2 Nv elektrodo įvandenilinimo efektas elektrolizės būdu ir H_2 dujose. Nustatyta, kad TiO_2 Nv – Cu_2O heterostruktūrai yra būdinga kur kas mažesnė priklausomybė nuo žadinimo šviesos kritimo kampo, kas galėtų būti ypač naudinga saulės elementų kontūruose. Ištirtos TiO_2 Nv, dekoruotų vario selenidų (Cu_3Se_2 ir $Cu_{2-x}Se$) nanodalelėmis, optinės savybės ir šviesos absorbcijos ypatumai. TiO_2 Nv plėvelių paviršiui ir nanovamzdeliams dekoruoti MoS_2 nanolapeliais optimizuota hidroterminio apdirbimo tirpalo sudėtis ir sąlygos. Tolygiam kristalinio MoS_2 suformavimui ant TiO_2 paviršiaus geriausiai tinka mažos koncentracijos amonio heptamolibdato ir tiourėjos tirpalai bei 220 – 225°C temperatūra. Nustatyta, kad Ti/TiO_2 Nv – MoS_2 elektrodai katalizuoja vandenilio išskyrimo iš rūgščių tirpalų reakciją ir pasižymi stabilumu.

Information about the author

Name, surname	Jelena Kovger
Birth date and place	6th of January 1987, Vilnius, Lithuania
Education 01/09/2006 - 30/06/2010	
2006-2010	Bachelor degree of Chemistry, Vilnius University
2010-2012	Master degree of Chemistry, Vilnius University
2012-2016	Doctoral studies at Institute of Chemistry of Centre for Physical Sciences and Technology
Work experience	
From 2016	Junior Research Assistant, Institute of Chemistry of Centre for Physical Sciences and Technology
2012-2016	Engineer, Institute of Chemistry of Centre for Physical Sciences and Technology

Informacija apie autorių

Vardas, pavardė	Jelena Kovger
Gimimo vieta ir data	1987 01 06, Vilnius, Lietuva
Išsilavinimas	
2006-2010	Chemijos bakalauro laipsnis, Vilniaus Universitetas
2010-2012	Chemijos magistro laipsnis, Vilniaus Universitetas
2012-2016	Doktorantūros studijos, Chemijos institutas, Fizinių ir technologijos mokslų centras
Darbo patirtis	
Nuo 2016	Jaunesnioji mokslo darbuotoja, Chemijos institutas, Fizinių ir technologijos mokslų centras
2012-2016	Inžinierė, Chemijos institutas, Fizinių ir technologijos mokslų centras